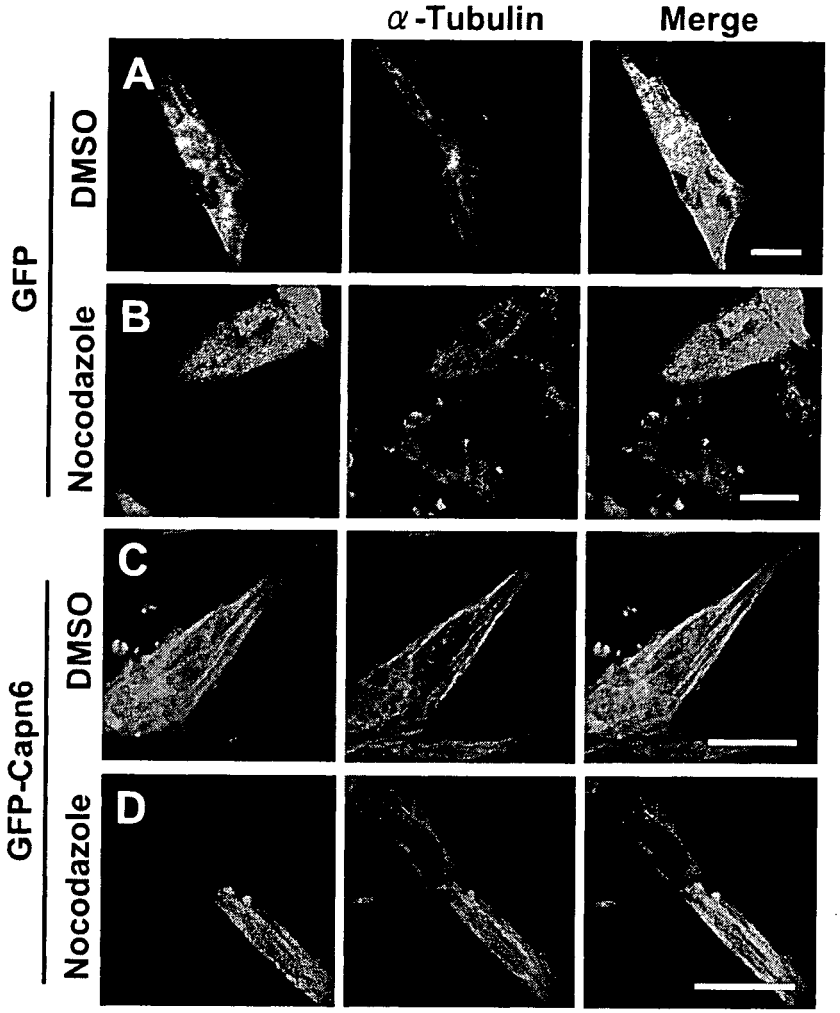

FIG. 4. GFP-Capn6 colocalizes to the microtubule network and induces microtubule bundling. NIH 3T3 cells were transfected with expression plasmids containing GFP (A and B) or GFP-Capn6 (C and D). After 16 h, the cells were treated with DMSO (vehicle) (A and C) or 500 nM nocodazole (B and D) for 15 min and stained with anti-GFP and anti-α-tubulin antibodies. GFP-Capn6 induced thick microtubule bundling (C), which was resistant to the destabilizing effect of nocodazole (D). The scale bars indicate 20 μm.

antibody against a synthetic oligopeptide corresponding to the C-terminal region of Capn6. This antibody recognized a band of ~74 kDa, corresponding to the expected molecular mass of Capn6, in untransfected cell lysates and more strongly in Capn6-transfected cell lysates (Fig. 5A), although it also detected several additional bands of unknown origin. The specificity of this ~74-kDa band was also confirmed by RNAi-mediated knockdown (see Fig. 8B).

To characterize the nature of Capn6 in terms of microtubule association, cell lysates were subjected to crude fractionation and Western blotting. Although microtubules are prone to depolymerization in the presence of 0.1% NP-40 at low temperature, MAP4, a protein associated with cold-stable microtubules (40), and a portion of acetylated α-tubulin were detected in the insoluble fraction (Fig. 5B). Capn1, a classical calpain localized in the cytoplasm, was found only in the soluble fraction (Fig. 5B). Under these conditions, Capn6 was predominantly detected in the insoluble fraction (Fig. 5B), which is consistent with the idea that Capn6 may associate with microtubules.

Correspondingly, immunostaining of NIH 3T3 cells with anti-Capn6 antibody detected signals mainly in the cytoplasm in a filamentous pattern, at least partially (Fig. 5C). This fine structure did not correlate with actin microfilaments visualized by rhodamine-labeled phalloidin (data not shown) but was largely superimposed on the intracellular microtubule network detected by anti-α-tubulin antibody (Fig. 5C). The correlation between Capn6 and microtubule signals was intensified in the presence of the microtubule-stabilizing agent paclitaxel (Fig. 5D). Conversely, treatment with nocodazole caused loss of the filamentous pattern of immunostaining and disrupted the colocalization between Capn6 and microtubules (Fig. 5E). In contrast to the predominant distribution of Capn6 to microtubules, Capn1 was localized in the cytoplasm with a granular pattern, although the signals could be partially overlapped with microtubules (Fig. 5F).

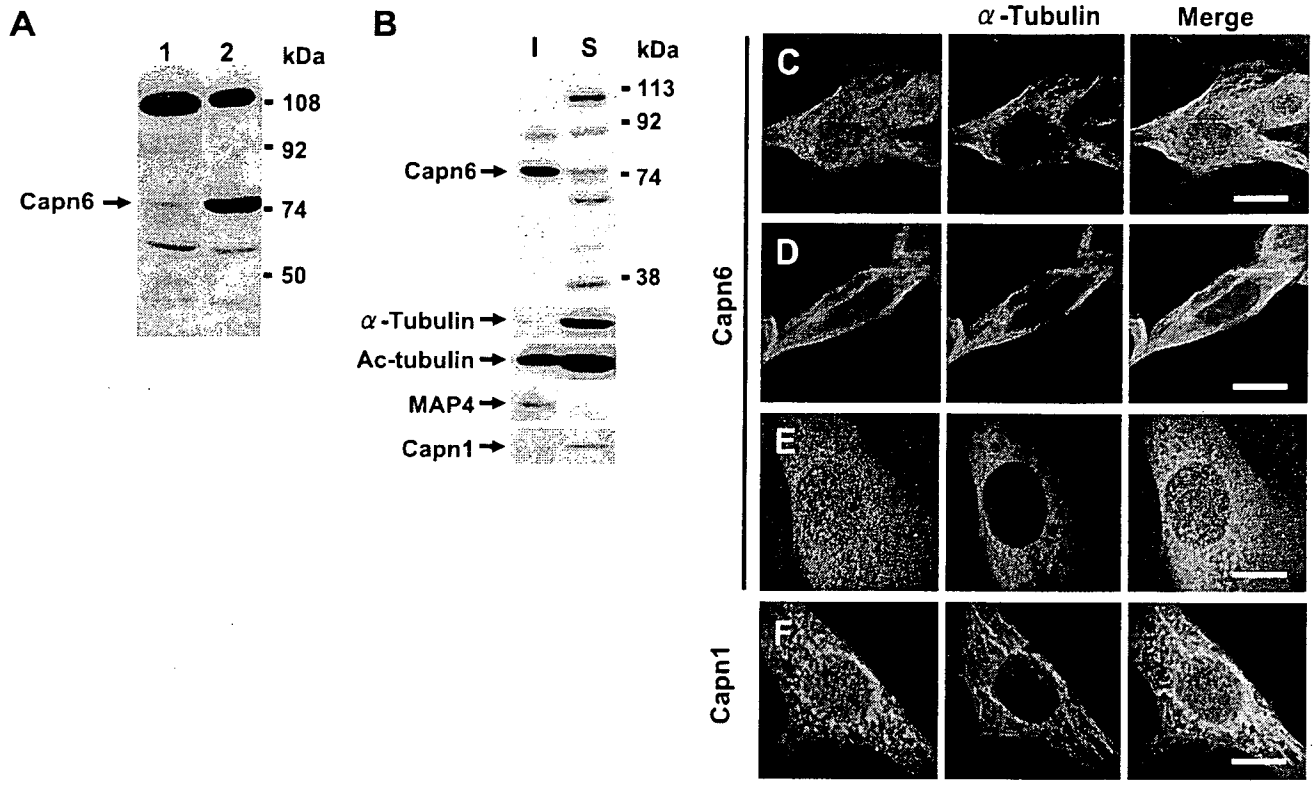

FIG. 5. Detection of Capn6 by rabbit polyclonal antibody. (A) Whole-cell lysates of untrasfected (lane 1) and Capn6-transfected (lane 2) NIH 3T3 cells were immunoblotted. The Capn6 antibody recognizes a band of ~74 kDa in untransfected cell lysates and more strongly in Capn6-transfected cell lysates. (B) NIH 3T3 cell lysates were separated into 0.1% NP-40-insoluble (lane I) and -soluble (lane S) fractions and immunoblotted with the indicated antibodies. The ~74-kDa band was found in the insoluble fraction with acetylated α-tubulin (Ac-tubulin) and MAP4. (C to F) Endogenous Capn6 colocalizes to the microtubule network. NIH 3T3 cells were treated with DMSO (vehicle) (C and F), 500 nM paclitaxel (D), or 500 nM nocodazole (E) for 30 min, and double stained with the anti-Capn6 (C to E) or anti-Capn1 (F) and anti-α-tubulin antibodies. The scale bars indicate 20 μm.

Capn6 interacts biochemically with microtubules. To test whether Capn6 can biochemically interact with microtubules, we performed a microtubule cosedimentation assay on NIH 3T3 cell lysate. After incubation of the cell lysate on ice for microtubule depolymerization, centrifugation yielded soluble supernatant containing monomerized tubulin. As shown in Fig. 6A, endogenous Capn6 was recovered in the microtubule-containing pellet in the presence of paclitaxel, although a large quantity of Capn6 remained in the supernatants. MAP4 also coprecipitated with microtubules in the pellet, whereas Capn1 remained in supernatants regardless of paclitaxel; these served as positive and negative controls, respectively (Fig. 6A). When GFP-Capn6 was overexpressed in NIH 3T3 cells, it was cosedimented with microtubules after the addition of paclitaxel, whereas it remained in the soluble fraction without paclitaxel treatment (Fig. 6B). In contrast, control GFP was not correlated with the amount of α-tubulin sedimented in the pellet, although a trace signal was detected in each lane (Fig. 6B).

The interaction between Capn6 and microtubules was further confirmed by a microtubule binding assay on filter paper and a GST pull-down assay. GST-Capn6 and unfused GST were run in SDS-PAGE, transferred to a PVDF filter, and then incubated with paclitaxel-stabilized microtubules. Immunoblotting with anti-tubulin antibody demonstrated that GST-Capn6, but not unfused GST, interacted with microtubules on the filter (Fig. 6C, lanes 1 and 2). MAP2, used as a positive control, also interacted with microtubules (Fig. 6C, lane 3). Furthermore, GST-Capn6, but not GST alone, pulled down paclitaxel-stabilized microtubules from NIH 3T3 cell lysates (Fig. 7C).

Domain III is responsible for Capn6-microtubule interaction. The structure of Capn6 protein consists of four domains (domains I, II, III, and T). To determine the domain(s) responsible for the interaction with microtubules, we constructed expression plasmids encoding GFP-tagged Capn6 deletion mutants (Fig. 7A) and transfected them into NIH 3T3 cells. In the presence of paclitaxel, GFP-tagged full-length Capn6 and Capn6(1-503), lacking domain T, colocalized to thickened microtubule bundles (Fig. 7B, a and b). In contrast, GFP-Capn6(1-326), lacking both domain III and domain T, did not colocalize to microtubules (Fig. 7B c). When individual domains were fused to GFP, only the construct containing domain III, GFP-Capn6(327-503), exhibited colocalization to microtubule bundles (Fig. 7B, d to g). Although domain III is sufficient for colocalization to microtubules, both 1-503 and 327-503 mutants did not induce multinucleation (data not shown), indicating that domain T is also necessary for full functional activity.

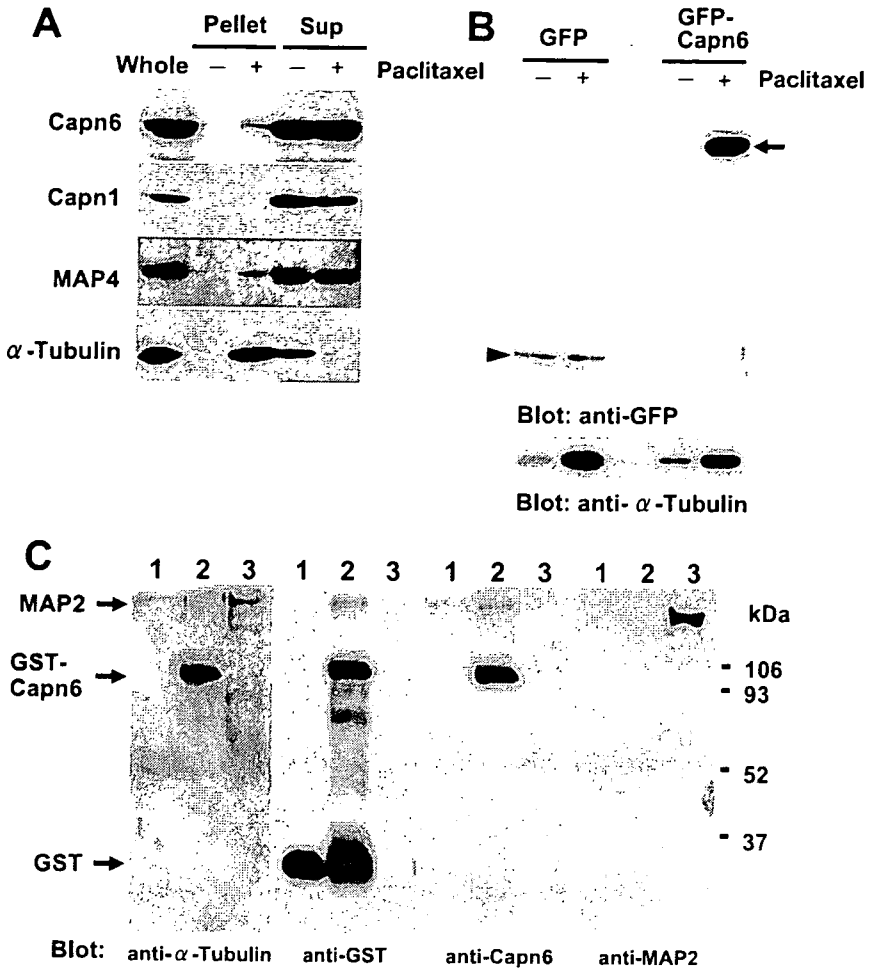

FIG. 6. Capn6 biochemically interacts with microtubules. (A and B) Lysates of untransfected (A) or GFP-Capn6-transfected (B) NIH 3T3 cells were subjected to microtubule cosedimentation assay. (A) Endogenous Capn6 was detected in the microtubule-containing pellet in the presence of paclitaxel, although a large quantity of Capn6 remained in the supernatants (Sup). MAP4 also coprecipitated with microtubules in the pellet, whereas Capn1, detected as autolytic products, remained in the supernatants regardless of the presence of paclitaxel. (B) Overexpressed GFP-Capn6 was recovered in the pellet in the presence of paclitaxel. In contrast, control GFP did not correlate with the amount of precipitated α-tubulin in the pellet. Arrow, GFP-Capn6; arrowhead, GFP. (C) Unfused GST (lane 1), GST fused to full-length Capn6 (lane 2), and purified MAP2 (lane 3) were subjected to a microtubule binding assay on filter paper. GST-Capn6 and MAP2 (positive control), but not unfused GST, bound to microtubules as detected by anti-α-tubulin antibody. The filter was sequentially reblotted with anti-GST, anti-Capn6, and anti-MAP2 antibodies to confirm the presence of intact proteins.

The association of each domain with microtubules was also examined by GST pull-down assay. GST-Capn6, but not unfused GST, pulled down paclitaxel-stabilized microtubules from NIH 3T3 cell lysates (Fig. 7C). Microtubules were also pulled down by GST-Capn6(327-503) (domain III) and GST-Capn6(504-641) (domain T), but not by GST-Capn6(1-56) (domain I) and GST-Capn6(57-326) (domain II) (Fig. 7C). Blotting with anti-acetylated α-tubulin revealed preferential binding of stabilized microtubules to domain III compared with domain T (Fig. 7C). These results suggest that the interaction of Capn6 with microtubules is mainly mediated by domain III, although domain T may also contribute to this association.

Suppression of Capn6 by siRNA destabilizes microtubules and affects actin organization. To investigate the role of endogenous Capn6 in the organization of the microtubule network, we used RNAi to selectively knock down Capn6 expression in NIH 3T3 cells. Stealth siRNAs targeting two different regions of the Capn6 transcript (nucleotides 1298 to 1322 and 1715 to 1739) downregulated Capn6 mRNA (Fig. 8A) and protein (Fig. 8B) to different extents. Immunostaining with anti-Capn6 antibody revealed the disappearance of microtubule-superimposed signals in Capn6-downregulated cells (Fig. 8C). In proportion to the extent of Capn6 downregulation, Capn6 siRNAs decreased the level of acetylated α-tubulin within the microtubule network of transfected cells (Fig. 8D). To confirm the effect of Capn6 downregulation on the microtubule organization, we introduced siRNAs into NIH 3T3 cells stably expressing GFP-tubulin. In Capn6 siRNA-transfected cells, the filamentous organization of the microtubule network was largely disrupted, resulting in relatively homogeneous distribution of GFP-tubulin with a preference for the perinuclear

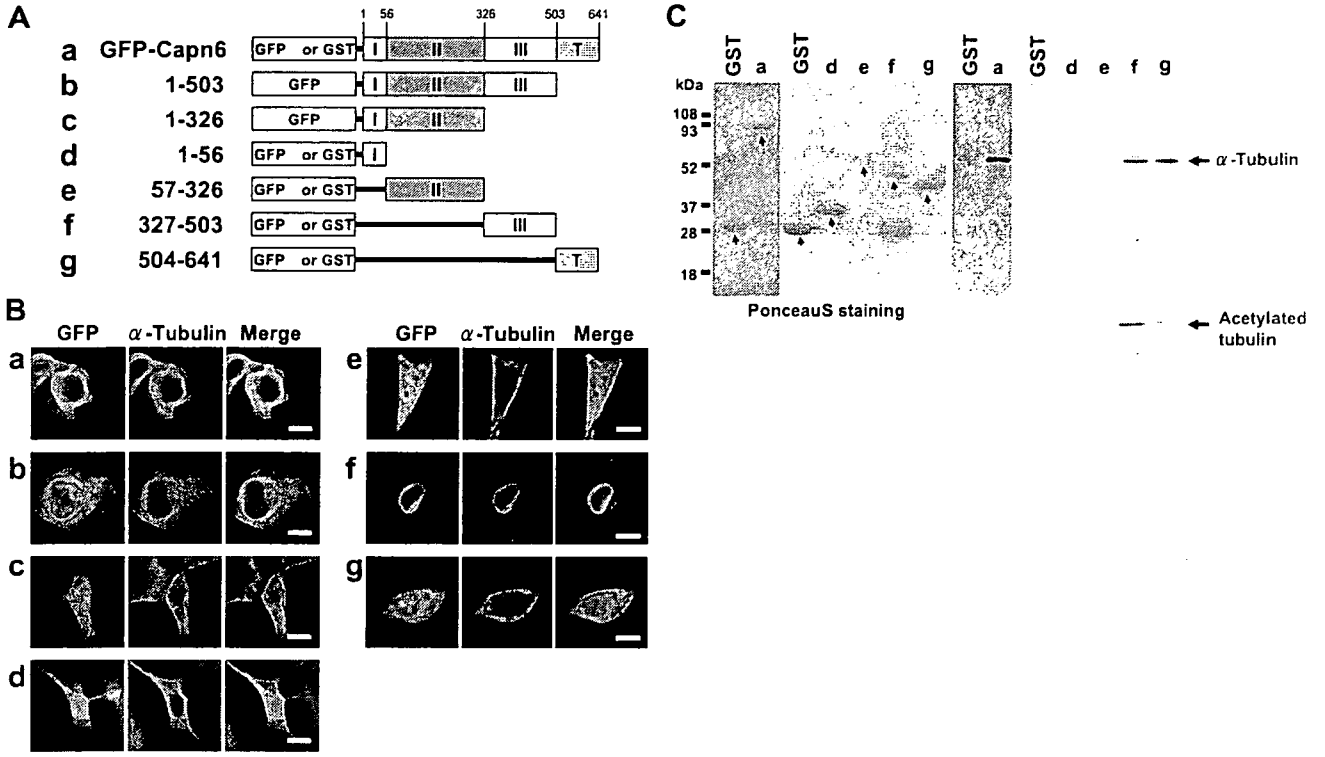

FIG. 7. Mapping of Capn6 domains interacting with microtubules. (A) Structures of GFP-tagged full-length Capn6 and its deletion mutants. (B) Localization of GFP-Capn6 mutants. NIH 3T3 cells were transfected with expression plasmids encoding GFP-Capn6 mutants, treated with 500 nM paclitaxel for 1 h, and stained with anti-GFP and anti-α-tubulin antibodies. Note that only GFP-Capn6 mutants containing domain III (amino acids 327 to 503) colocalized to microtubule bundles. The scale bars indicate 20 μm. (C) GST pull-down assay for microtubule binding. Microtubules were detected by anti-α-tubulin and anti-acetylated tubulin antibodies. α-Tubulin was pulled down from NIH 3T3 cell lysates by GST–full-length Capn6, GST-Capn6(327-503) (domain III), and GST-Capn6(504-641) (domain T), but not by GST-Capn6(1-56) (domain I), GST-Capn6(57-326) (domain II), or GST alone (right). Blotting with anti-acetylated tubulin showed that stable microtubules were more likely to bind to domain III than to domain T. The amounts of GFP fusion proteins were grossly estimated by Ponceau staining (left). The arrows indicate GST fusion proteins.

region (Fig. 8E). Decreases in acetylated-α-tubulin levels in Capn6-downregulated cells were also confirmed by Western blotting analysis (Fig. 8F).

To further analyze the functional consequences of Capn6 downregulation, we examined cellular behavior during cytokinesis in control and Capn6 siRNA-transfected cells using time-lapse microscopy. After the onset of anaphase, cleavage furrow formation and progression occurred normally in Capn6-downregulated cells, as well as in control cells (Fig. 9A and B). At subsequent stages, Capn6-downregulated cells tended to form lamellipodial protrusions with ruffling and to become flat much earlier than control cells (Fig. 9A and B). When the times from anaphase onset to the first appearance of lamellipodial protrusions from round dividing cells were compared, it was significantly shorter in Capn6-downregulated cells than in control cells (Fig. 9C). In contrast, the time from anaphase onset to the completion of cell abscission was not significantly different between control and Capn6-downregulated cells (Fig. 9D).

Time-lapse microscopy also showed that cell motility was increased in Capn6-downregulated cells, in which lamellipodial ruffling was very prominent (Fig. 10A and B; see Videos S4 to S6 in the supplemental material). Changes in actin organization associated with lamellipodium formation were confirmed by staining with rhodamine-phalloidin (Fig. 10C). These observations suggest that silencing of Capn6 may facilitate dynamic instability of microtubules and actin reorganization in NIH 3T3 cells.

DISCUSSION

In the present study, we first identified Capn6 as a downstream molecule of ET-1 signaling in pharyngeal-arch development. Subsequent analysis has demonstrated that Capn6 is a functional protein with microtubule-associated activities. Overexpression of Capn6 stimulated the formation of microtubule bundles and interrupted cytokinesis, resulting in multinucleation. Capn6 colocalized to the microtubule structures, including the central spindle and midbody, during cytokinesis. The interaction between Capn6 and microtubules was also confirmed by biochemical analysis. This interaction appeared to be mainly mediated by domain III, a C2-like domain. Finally, RNAi-mediated Capn6 inactivation caused disruption of the microtubule organization with loss of acetylated α-tubulin, affecting actin organization and cell motility.

Microtubules are filamentous polymers constituted of α- and β-tubulin that are engaged in many cellular functions, includ-

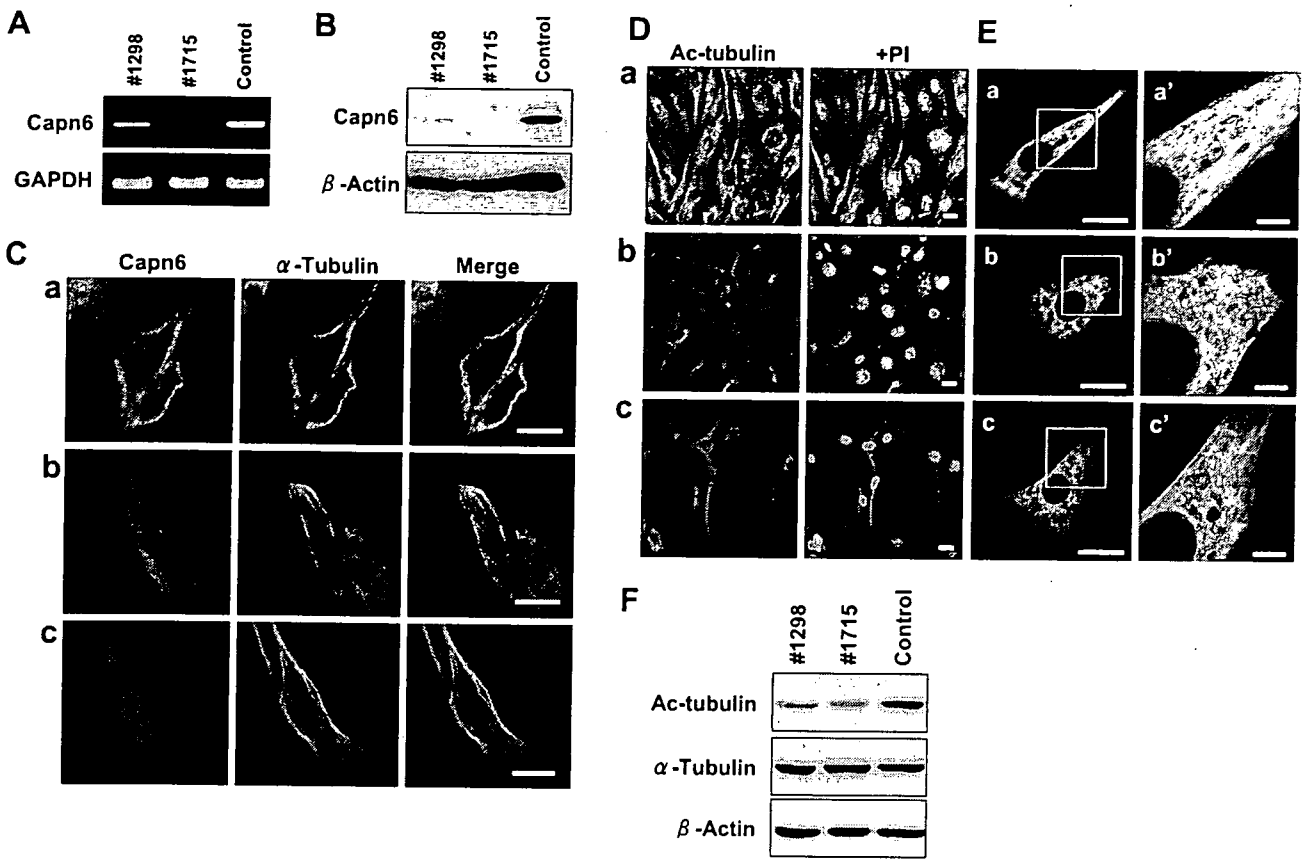

FIG. 8. RNAi-mediated inactivation of Capn6 destabilizes microtubules. NIH 3T3 cells were transfected with Capn6-targeted or control siRNAs. Forty-eight hours after transfection, the effects of siRNAs were evaluated. (A and B) RT-PCR for Capn6 mRNA (A) and Western blotting for Capn6 protein (B). Stealth siRNAs targeting two different regions of the Capn6 transcript (1298 and 1715 for nucleotides 1298 to 1322 and 1715 to 1739, respectively) downregulated Capn6 mRNA and protein levels. (C) Immunostaining with anti-Capn6 antibody. Signals superimposed on microtubules were evident in paclitaxel-treated control siRNA-transfected cells (a), but not in paclitaxel-treated cells transfected with 1298 (b) or 1715 (c) siRNA, although background cytosolic staining was comparable in the three groups. (D) NIH 3T3 cells were transfected with control (a), 1298 (b), or 1715 (c) siRNA and immunostained for acetylated α-tubulin (Ac-tubulin). The levels of acetylated α-tubulin decreased in cells transfected with Capn6-targeted siRNA. (E) NIH 3T3 cells stably expressing GFP-tubulin were transfected with control (a), 1298 (b), or 1715 (c) siRNA and immunostained for GFP. a′, b′, and c′ are magnified images of the boxed areas in a, b, and c, respectively. Microtubule network structures were largely disrupted in cells transfected with Capn6-targeted siRNA. The scale bars indicate 20 μm (C, D, and a to c in panel E) and 5 μm (a′ to c′ in panel E). (F) Western blotting of control and Capn6 siRNA-transfected NIH 3T3 cell extracts with anti-acetylated α-tubulin, anti-α-tubulin, and anti-β-actin antibodies. Acetylated α-tubulin levels decreased in Capn6 siRNA (1298 and 1715)-transfected cells compared with control siRNA-transfected cells, whereas total α-tubulin levels did not decrease. Blotting for β-actin served as an internal control. Similar results were obtained in three independent experiments. Representative data are shown.

ing cell division, cell shape integration, and organelle transport. The dynamic instability involving polymerization-depolymerization cycles is regulated by microtubule-associated proteins (MAPs), such as MAP1, MAP2, and tau, in neural cells and is critical for the function of microtubules. Many previous reports have demonstrated that the classical calpains can cleave tubulin and MAPs under in vitro conditions (11). However, little is known about the physiological role of the calpain system in the regulation of microtubule dynamics. Recently, several studies have implicated the calpain-induced proteolysis of MAPs in the pathogenesis of neurodegenerative disorders, including Alzheimer's disease (12), and the role of the calpain system in microtubule organization is now an issue of growing concern. In this context, the present findings may provide new insight into this issue by demonstrating that the protease-deficient calpain can associate with and stabilize microtubules.

Preferential distribution to the microtubule network is highly characteristic of Capn6 among the calpain family members. Capn1, for example, is homogeneously distributed in the cytoplasm and is translocated to the plasma membrane upon an increase in cytosolic Ca^{2+} (8). Lane et al. reported that Capn1 is distributed through the cytoplasm in a fibrillar form, reminiscent of the cytoskeletal architecture (24). In our present study, however, Capn1 was detected in the 0.1% NP-40-soluble fraction and distributed in a rather granular form in NIH 3T3 cells. Capn2, another classical calpain, also localizes in the cytoplasm in a diffuse or fine granular form (24). No other calpains have been shown to be associated with microtubules.

The interaction between Capn6 and microtubules appears to be mediated mainly by domain III. In Capn1 and Capn2, domain III constitutes a pair of four-stranded antiparallel

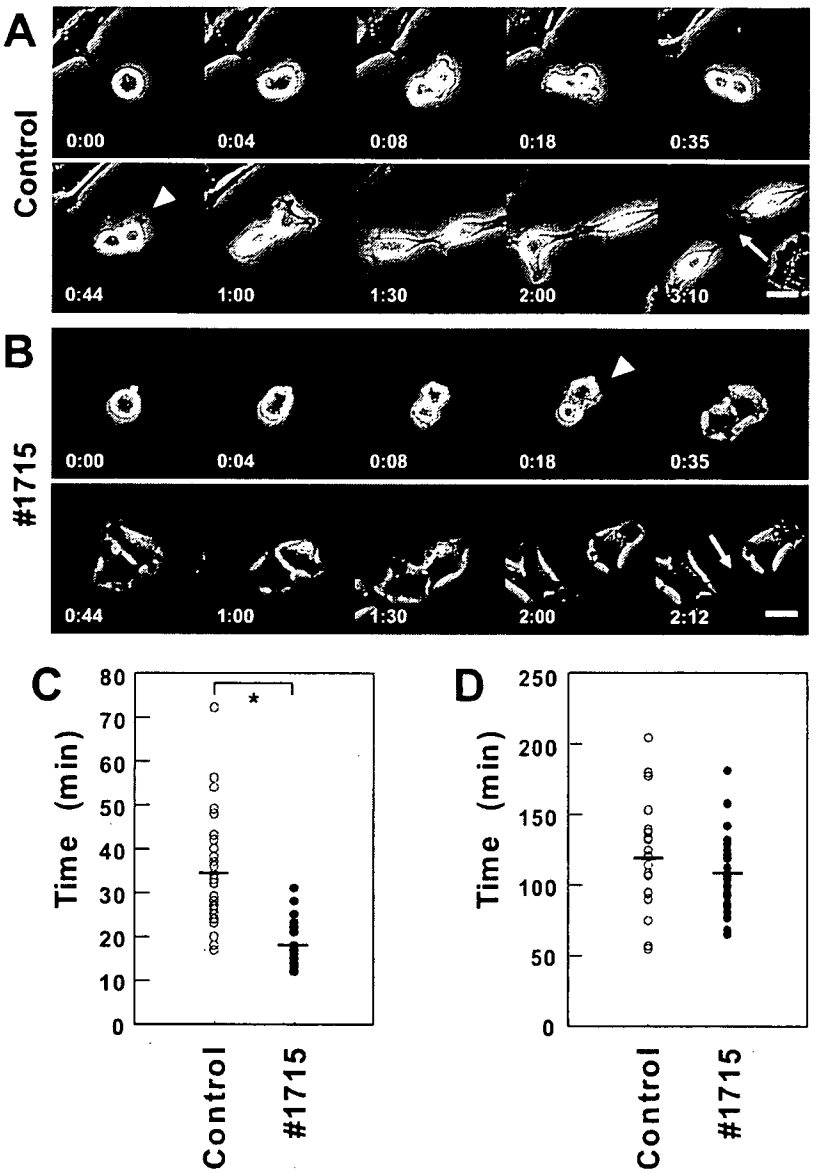

FIG. 9. RNAi-mediated inactivation of Capn6 affects cytoskeletal reorganization during cytokinesis. (A and B) Representative images from time-lapse recordings of control (A) and Capn6 (B) siRNA-transfected NIH 3T3 cells. Cleavage furrows were similarly formed after anaphase onset in control and Capn6 siRNA (1715)-transfected cells. At subsequent stages, Capn6 siRNA-transfected cells tended to form lamellipodial protrusions with ruffling and to become flat much earlier than control cells. Times are in h/min after anaphase onset (0:00 time point). Arrowheads, first appearance of lamellipodial protrusion; arrows, completion of cell abscission. The scale bars indicate 20 μm. (C) Comparison of the times from anaphase onset to the first appearance of lamellipodial protrusions. The time was significantly shorter in Capn6-downregulated cells (17.9 [mean] ± 4.5 [standard deviation] min; $n = 30$) than in control cells (34.4 ± 12.4 min; $n = 30$). *, $P < 0.0001$; Mann-Whitney nonparametric test. (D) Comparison of the times from anaphase onset to the completion of cell abscission. No significant difference was observed between control cells (118.8 ± 35.1 min; $n = 25$) and Capn6-downregulated cells (108.6 ± 27.6 min; $n = 24$).

β-sheets (15, 30, 37), like the C2 domain, a Ca^{2+}- and phospholipid-binding module (33). Although the function of this domain is unclear, previous reports have indicated its roles in the regulation of Ca^{2+} sensitivity of the enzyme (14, 15) and in Ca^{2+}-dependent translocation to the cell membrane (8). Domain III of Capn6 (amino acids 327 to 503) shows similarity to that of Capn2, with only 28% amino acid identity, as revealed by a BLAST search (data not shown), suggesting limited conservation of the domain structure. In addition, domain III of Capn6 lacks sequences corresponding to the conserved acidic loop to form interdomain salt bridges important for Ca^{2+} sensitivity (13). Thus, this domain may be unusual in structure and function in the calpain family.

In addition to colocalization to microtubules, Capn6 causes the formation of microtubule bundles. Increased acetylated α-tubulin contents in Capn6-induced microtubule bundles and resistance to nocodazole suggest that Capn6 has a microtubule-stabilizing property. Furthermore, disruption of microtu-

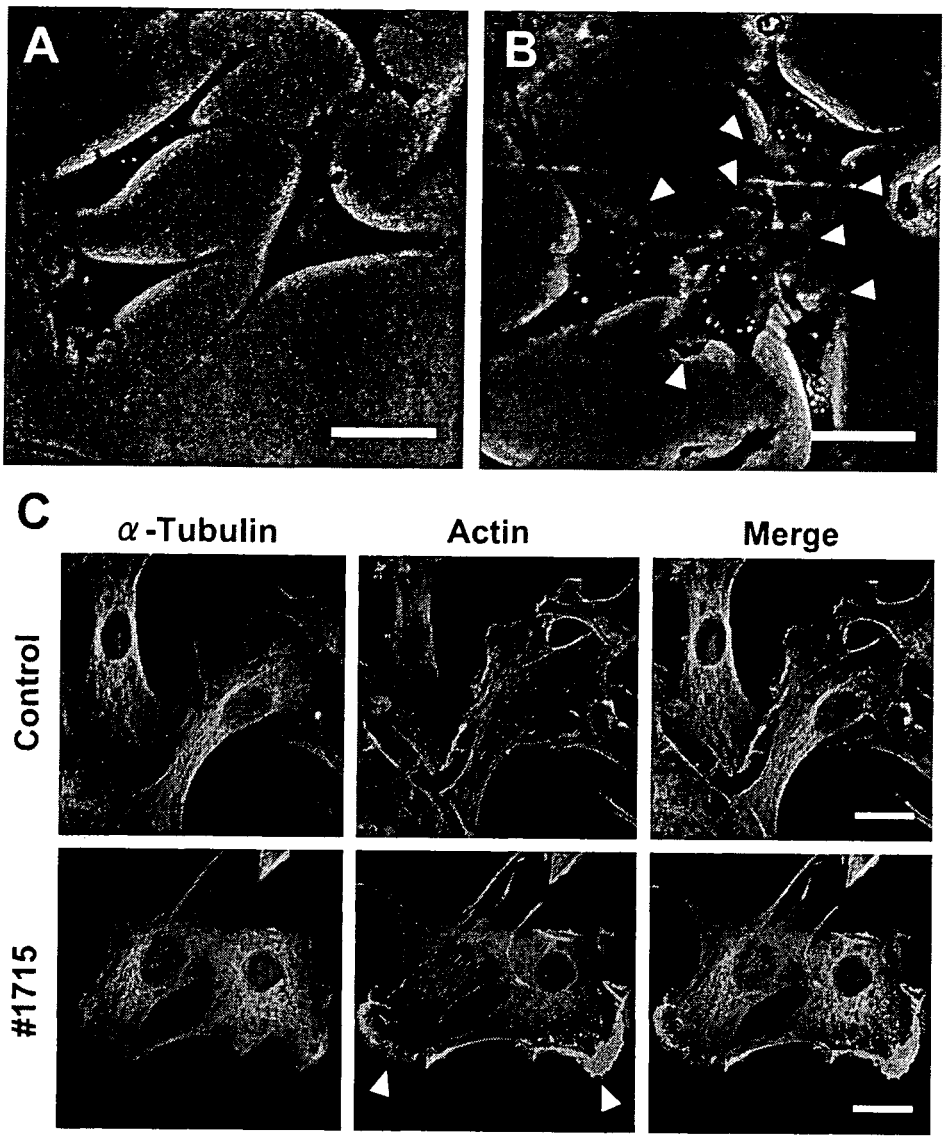

FIG. 10. RNAi-mediated inactivation of Capn6 induces lamellipodium formation. (A and B) Phase-contrast micrographs of control (A) and Capn6 (B) siRNA-transfected NIH 3T3 cells. Capn6 siRNA(1715)-transfected cells demonstrated enhanced lamellipodium formation with membrane ruffling (arrowheads). (C) Double staining of control and Capn6(1715) siRNA-transfected NIH 3T3 cells with anti-tubulin and rhodamine-phalloidin. Capn6 siRNA-transfected cells demonstrate the assembly of actin filaments in lamellipodia (arrowheads). The scale bars indicate 20 μm.

bule bundles and decrease in acetylated α-tubulin levels by RNAi-mediated Capn6 inactivation indicate the role of endogenous Capn6 in the maintenance of stable microtubule architecture.

The Capn6-induced disruption of cytokinesis may be a consequence of its stabilizing effect on microtubules. In Capn6-overexpressing cells, the cleavage furrow was created along with chromosomal separation with an expected time course, but furrow ingression was retarded thereafter, suggesting that Capn6 functioned at the late stage of cytokinesis. During the process of cytokinesis, overexpressed Capn6 colocalized to the central spindle of the midzone and to the whole midbody, where Capn6 may affect the progression and completion of cytokinesis. Cytokinesis is elaborately controlled at several steps involving various molecules concentrating at the midbody (10). Changes in microtubule stability might interrupt such cytokinetic machinery, leading to disrupted cytokinesis in Capn6-overexpressing cells. Another possible explanation is that stabilization of microtubules by Capn6 may prevent the cytoskeletal reorganization required for cell division, although the molecular network underlying this process remains largely unknown. Correspondingly, Capn6 siRNA transfection resulted in the early appearance of lamellipodial protrusions during cytokinesis, indicating that cytoskeletal reorganization may be facilitated by Capn6 inactivation.

The observation that siRNA-mediated Capn6 inactivation

enhanced the formation of lamellipodia with membrane ruffling is also consistent with the involvement of Capn6 in microtubule stability. Previous reports have demonstrated that changes in microtubule stability affect cell motility through microtubule-actin interactions (34). For example, Hubbert et al. have shown that deacetylation of α-tubulin by HDAC6 promotes chemotactic cell migration (17). Waterman-Storer et al. have provided a model in which the growth phase of microtubule dynamic instability drives actin polymerization and lamellipodial protrusion via Rac1 activation (39). Taken together with these findings, the present results suggest that Capn6 may be involved in the control of microtubule dynamic instability and actin organization.

How can Capn6 induce microtubule stabilization? It is unlikely that Capn6 has a concealed protease activity by which it may modulate microtubule dynamics, because calpain inhibitors did not inhibit Capn6-induced microtubule bundling. Rather, Capn6 may exert its effect by antagonizing other calpains as a nonproteolytic family member. Indeed, the stability of microtubules is enhanced by MAPs (6, 18), which are in vitro calpain substrates. Rho GTPase, another possible calpain substrate (20), and its effector, mDia, also have microtubule-stabilizing properties (3, 31). It would be worthwhile to test whether Capn6 may protect these microtubule-stabilizing factors from proteolysis in the restricted cytoskeletal regions. It is also possible that Capn6 may stabilize microtubules through an as-yet-unknown function independent of protease activity. For example, the pattern of microtubule bundling may suggest possible interactions between Capn6 and other signaling pathways. Capn6-transfected cells exhibited stable microtubule bundling predominantly in the perinuclear region. Remarkably, a similar pattern of microtubule bundling is induced by certain members of sterile 20 (STE20)-like kinases. *Xenopus* p21-activated kinase 5 (X-PAK5), a Cdc42/Rac effector, colocalizes to microtubules and promotes the formation of stable microtubule bundles around the nucleus (1). Prostate-derived STE20-like kinase, a member of the germinal-center kinase-like kinase subfamily, also produces perinuclear microtubule bundles (27). These kinases are also involved in the regulation of actin organization, suggesting that they may play roles in the cross talk between microtubules and the actin cytoskeleton. Although the role of Capn6 in the regulation of actin organization has not yet been determined, the enhanced lamellipodium formation induced by Capn6 silencing may suggest the possible involvement of Capn6 in this cytoskeletal cross talk.

Is Capn6 involved in embryogenesis through its microtubule-stabilizing effect? The answer to this question remains unknown, although Capn6 was identified as a molecule in the genetic hierarchy controlling pharyngeal-arch development. In this respect, it is noteworthy that cytoskeletal remodeling, including microtubules, is involved in various processes during animal development. For example, Rho family GTPase-regulating proteins required for cytokinesis have also emerged as modulators of cytoskeletal reorganization in transitions between the epithelium and mesenchyme in either direction (23). It is possible that Capn6, expressed in the pharyngeal-arch epithelium and mesenchyme, participates in developmental processes involving cytoskeletal reorganization in cooperation with these proteins. Further investigations using a gene-targeting approach are expected to clarify the link between the molecular functions of Capn6 and developmental processes.

ACKNOWLEDGMENTS

We thank Hideyuki Saya (Kumamoto University), Yoshimitsu Kanai, and Yasuko Noda (The University of Tokyo) for technical advice and helpful discussion. K.T. is a Research Fellow of the Japan Society for the Promotion of Science (DC1).

This work was supported by grants from the Japan Society for the Promotion of Science Research for the Future Program; grants-in-aid for scientific research from the Ministry of Education, Culture, Sports, Science and Technology, Japan; and a Research Grant from the Uehara Memorial Foundation.

REFERENCES

1. **Cau, J., S. Faure, M. Comps, C. Delsert, and N. Morin.** 2001. A novel p21-activated kinase binds the actin and microtubule networks and induces microtubule organization. J. Cell Biol. **155**:1029–1042.
2. **Clouthier, D. E., K. Hosoda, J. A. Richardson, S. C. Williams, H. Yanagisawa, T. Kuwaki, M. Kumada, R. E. Hammer, and M. Yanagisawa.** 1998. Cranial and cardiac neural crest defects in endothelin-A receptor-deficient mice. Development **125**:813–824.
3. **Cook, T. A., T. Nagasaki, and G. G. Gundersen.** 1998. Rho guanosine triphosphatase mediates the selective stabilization of microtubules induced by lysophosphatidic acid. J. Cell Biol. **141**:175–185.
4. **Dear, N., K. Matena, M. Vingron, and T. Boehm.** 1997. A new subfamily of vertebrate calpains lacking a calmodulin-like domain: implications for calpain regulation and evolution. Genomics **45**:175–184.
5. **Dear, T. N., and T. Boehm.** 1999. Diverse mRNA expression patterns of the mouse calpain genes Capn5, Capn6 and Capn11 during development. Mech. Dev. **89**:201–209.
6. **Drewes, G., A. Ebneth, and E.-M. Mandelkow.** 1998. MAPs, MARKs and microtubule dynamics. Trends Biochem. Sci. **23**:307–311.
7. **Fukuhara, S., Y. Kurihara, Y. Arima, N. Yamada, and H. Kurihara.** 2004. Temporal requirement of signaling cascade involving endothelin-1/endothelin A receptor in branchial arch development. Mech. Dev. **121**:1223–1233.
8. **Gil-Parrado, S., O. Popp, T. A. Knoch, S. Zahler, F. Bestvater, M. Felgentrager, A. Holloschi, A. Fernandez-Montalvan, E. A. Auerswald, H. Fritz, P. Fuentes-Prior, W. Machleidt, and E. Spiess.** 2003. Subcellular localization and in vivo subunit interactions of ubiquitous μ-calpain. J. Biol. Chem. **278**:16336–16346.
9. **Glading, A., D. A. Lauffenburger, and A. Wells.** 2002. Cutting to the chase: calpain proteases in cell motility. Trends Cell Biol. **12**:46–54.
10. **Glotzer, M.** 2005. The molecular requirements for cytokinesis. Science **307**: 1735–1739.
11. **Goll, D. E., V. F. Thompson, H. Li, W. Wei, and J. Cong.** 2003. The calpain system. Physiol. Rev. **83**:731–801.
12. **Higuchi, M., N. Iwata, and T. C. Saido.** 2005. Understanding molecular mechanisms of proteolysis in Alzheimer's disease: progress toward therapeutic interventions. Biochim. Biophys. Acta **1751**:60–67.
13. **Hosfield, C. M., J. S. Elce, P. L. Davies, and Z. Jia.** 1999. Crystal structure of calpain reveals the structural basis for Ca^{2+}-dependent protease activity and a novel mode of enzyme activation. EMBO J. **18**:6880–6889.
14. **Hosfield, C. M., T. Moldoveanu, P. L. Davies, J. S. Elce, and Z. Jia.** 2001. Calpain mutants with increased Ca^{2+} sensitivity and implications for the role of the C_2-like domain. J. Biol. Chem. **276**:7404–7407.
15. **Hosfield, C. M, J. S. Elce, and Z. Jia.** 2004. Activation of calpain by Ca^{2+}: roles of the large subunit N-terminal and domain III-IV linker peptides. J. Mol. Biol. **343**:1049–1053.
16. **Huang, Y., and K. K. Wang.** 2001. The calpain family and human disease. Trends Mol. Med. **7**:355–362.
17. **Hubbert, C., A. Guardiola, R. Shao, Y. Kawaguchi, A. Ito, A. Nixon, M. Yoshida, X. F. Wang, and T. P. Yao.** 2002. HDAC6 is a microtubule-associated deacetylase. Nature **417**:455–458.
18. **Kaech, S., B. Ludin, and A. Matus.** 1996. Cytoskeletal plasticity in cells expressing neuronal microtubule-associated proteins. Neuron **17**:1189–1199.
19. **Kimmel, C. B., B. Ullmann, M. Walker, C. T. Miller, and J. G. Crump.** 2003. Endothelin 1-mediated regulation of branchial bone development in zebrafish. Development **130**:1339–1351.
20. **Kulkarni, S., D. E. Goll, and J. E. Fox.** 2002. Calpain cleaves RhoA generating a dominant-negative form that inhibits integrin-induced actin filament assembly and cell spreading. J. Biol. Chem. **277**:24435–24441.
21. **Kurihara, Y., H. Kurihara, H. Suzuki, T. Kodama, K. Maemura, R. Nagai, H. Oda, T. Kuwaki, W.-H. Cao, N. Kamada, K. Jishage, Y. Ouchi, S. Azuma, Y. Toyoda, T. Ishikawa, M. Kumada, and Y. Yazaki.** 1994. Elevated blood pressure and craniofacial abnormalities in mice deficient in endothelin-1. Nature **368**:703–710.
22. **Kurihara, Y., H. Kurihara, H. Oda, K. Maemura, R. Nagai, T. Ishikawa, and**

Y. Yazaki. 1995. Aortic arch malformations and ventricular septal defect in mice deficient in endothelin-1. J. Clin. Investig. 96:293–300.
23. Labouesse, M. 2004. Epithelium-mesenchyme: a balancing act of RhoGAP and RhoGEF. Curr. Biol. 14:R508–R510.
24. Lane, R. D., D. M. Allan, and R. L. Mellgren. 1992. A comparison of the intracellular distribution of μ-calpain, m-calpain, and calpastatin in proliferating human A431 cells. Exp. Cell Res. 203:5–16.
25. Masaki, T. 2004. Historical review: endothelin. Trends Pharmacol. Sci. 25: 219–224.
26. Matena, K., T. Boehm, and N. Dear. 1998. Genomic organization of mouse Capn5 and Capn6 genes confirms that they are a distinct calpain subfamily. Genomics 48:117–120.
27. Mitsopoulos, C., C. Zihni, R. Garg, A. J. Ridley, and J. D. H. Morris. 2003. The prostate-derived sterile 20-like kinase (PSK) regulates microtubule organization and stability. J. Biol. Chem. 278:18085–18091.
28. Nakaseko, Y., K. Nabeshima, K. Kinoshita, and M. Yanagida. 1996. Dissection of fission yeast microtubule associating protein $p93^{Dis1}$: regions implicated in regulated localization and microtubule interaction. Genes Cells 1:633–644.
29. Ozeki, H., Y. Kurihara, K. Tonami, S. Watatani, and H. Kurihara. 2004. Endothelin-1 regulates the dorsoventral branchial arch patterning in mice. Mech. Dev. 121:387–395.
30. Pal, G. P., T. De Veyra, J. S. Elce, and Z. Jia. 2003. Crystal structure of a micro-like calpain reveals a partially activated conformation with low Ca^{2+} requirement. Structure 11:1521–1526.
31. Palazzo, A. F., T. A. Cook, A. S. Alberts, and G. G. Gundersen. 2001. mDia mediates Rho-regulated formation and orientation of stable microtubules. Nat. Cell Biol. 3:723–729.
32. Piperno, G., M. LeDizet, and X. J. Chang. 1987. Microtubules containing acetylated alpha-tubulin in mammalian cells in culture. J. Cell Biol. 104:289–302.
33. Rizo, J., and T. C. Südhof. 1998. C_2-domains, structure and function of a universal Ca^{2+}-binding domain. J. Biol. Chem. 273:15879–15882.
34. Rodriguez, O. C., A. W. Schaefer, C. A. Mandato, P. Forscher, W. M. Bement, and C. M. Waterman-Storer. 2003. Conserved microtubule-actin interactions in cell movement and morphogenesis. Nat. Cell Biol. 5:599–609.
35. Sorimachi, H., S. Ishiura, and K. Suzuki. 1997. Structure and physiological function of calpains. Biochem. J. 328:721–732.
36. Sorimachi, H., and K. Suzuki. 2001. The structure of calpain. J. Biochem. (Tokyo) 129:653–664.
37. Strobl, S., C. Fernandez-Catalan, M. Braun, R. Huber, H. Masumoto, K. Nakagawa, A. Irie, H. Sorimachi, G. Bourenkow, H. Bartunik, K. Suzuki, and W. Bode. 2000. The crystal structure of calcium-free human m-calpain suggests an electrostatic switch mechanism for activation by calcium. Proc. Natl. Acad. Sci. USA 97:588–592.
38. Suzuki, K., and H. Sorimachi. 1998. A novel aspect of calpain activation. FEBS Lett. 433:1–4.
39. Waterman-Storer, C. M., R. A. Worthylake, B. P. Liu, K. Burridge, and E. D. Salmon. 1999. Microtubule growth activates Rac1 to promote lamellipodial protrusion in fibroblasts. Nat. Cell Biol. 1:45–50.
40. Webster, D. R., and J. M. Bratcher. 2006. Developmental regulation of cardiac MAP4 protein expression. Cell Motil. Cytoskeleton 63:512–522.
41. Wilkinson, D. 1992. *In situ* hybridisation: a practical approach. IRL Press, Oxford, United Kingdom.
42. Yanagisawa, M., H. Kurihara, S. Kimura, Y. Tomobe, M. Kobayashi, Y. Mitsui, Y. Yazaki, K. Goto, and T. Masaki. 1988. A novel potent vasoconstrictor peptide produced by vascular endothelial cells. Nature 332:411–415.

ELSEVIER

Atherosclerosis 196 (2008) 391–397

ATHEROSCLEROSIS

www.elsevier.com/locate/atherosclerosis

A novel method for evaluating human carotid artery elasticity: Possible detection of early stage atherosclerosis in subjects with type 2 diabetes

Hisashi Okimoto[a,1], Yasushi Ishigaki[a,1], Yoshihiro Koiwa[b], Yoshinori Hinokio[a], Takehide Ogihara[c], Susumu Suzuki[a], Hideki Katagiri[c,f], Takayoshi Ohkubo[d,f], Hideyuki Hasegawa[e], Hiroshi Kanai[e], Yoshitomo Oka[a,g,*]

[a] *Division of Molecular Metabolism and Diabetes, Tohoku University Graduate School of Medicine, Japan*
[b] *Division of Cardiovascular Medicine, Tohoku University Graduate School of Medicine, Japan*
[c] *Division of Advanced Therapeutics for Metabolic Diseases, Tohoku University Graduate School of Medicine, Japan*
[d] *Department of Planning for Drug Development and Clinical Evaluation, Tohoku University Graduate School of Pharmaceutical Science and Medicine, Japan*
[e] *Department of Electrical Engineering, Tohoku University Graduate School of Engineering, Japan*
[f] *The 21st Century COE Programs, Comprehensive Research and Education Center for Planning of Drug Development and Clinical Evaluation, Japan*
[g] *The 21st Century COE Programs, Center for Innovative Therapeutic Development towards the Conquest of Signal Transduction Diseases, Tohoku University, Sendai, Japan*

Received 29 March 2006; received in revised form 5 September 2006; accepted 12 November 2006
Available online 18 December 2006

Abstract

We recently developed a novel method for evaluating the elasticity of arterial walls, the phased tracking method. Herein, we evaluated atherosclerosis of the carotid artery with this method in 242 individuals with type 2 diabetes. In multiple regression analysis of subject status, age, systolic blood pressure and hyperlipidemia were found to be independently associated with carotid artery elasticity values. We also measured currently established values for atherosclerosis, carotid artery IMT and baPWV, in these subjects. Carotid artery elasticity correlated with max IMT ($r=0.291$, $p<0.01$), plaque score (PS) ($r=0.220$, $p<0.01$) and baPWV ($r=0.345$, $p<0.01$). Elasticity, max IMT and plaque score, all correlated with the number of risk factors for atherosclerosis, i.e. hypertension, hyperlipidemia and smoking, in addition to diabetes, consistent with the view that these values reflect atherosclerosis. Importantly, however, in subjects with IMT <1.1 mm, who are classified as not having atherosclerosis as defined by IMT criteria, only carotid artery elasticity correlated with the number of risk factors ($p<0.05$). These results suggest that (1) the measured carotid artery elasticity values reflect atherosclerosis and (2) our novel method has potential for detecting atherosclerosis in its early stage.

Keywords: Human carotid artery elasticity; Atherosclerosis; Diabetes

1. Introduction

Individuals with type 2 diabetes are at very high risk for atherosclerosis [1]. Although many methods have been developed for detecting atherosclerosis, those currently available are mainly for detecting established atherosclerosis. Therefore, the disease process is well-advanced at the time of diagnosis. To reduce future cardiovascular complications in subjects with atherogenic disorders such as type 2 diabetes

* Corresponding author at: Division of Molecular Metabolism and Diabetes, Tohoku University Graduate School of Medicine, 2-1 Seiryo-machi, Aoba-ku, Sendai 980-8575, Japan. Tel.: +81 22 717 7611; fax: +81 22 717 7611.
E-mail address: oka-y@mail.tains.tohoku.ac.jp (Y. Oka).
[1] These authors contributed equally to this work.

0021-9150/$ – see front matter © 2006 Elsevier Ireland Ltd. All rights reserved.
doi:10.1016/j.atherosclerosis.2006.11.020

mellitus, detection of early stage atherosclerosis is urgently needed.

Carotid intima-media thickness (IMT) is a well-established surrogate marker for cardiovascular risk [2]. Measuring IMT with ultrasonography is non-invasive and relatively simple [3,4], and IMT is now commonly employed as an endpoint marker in clinical trials. Carotid IMT correlates with cardiovascular risk factors and indeed predicts macrovascular events such as myocardial infarction [5] and stroke [6]. Carotid IMT is greater in subjects with diabetes, both type 1 [7] and type 2 [8,9], than in non-diabetic subjects of the same age. When analyzed in diabetic patients, IMT correlates with glycemic control and the duration of diabetes. Interventions, such as blood glucose lowering [10], lipid lowering [11], ACE inhibition [12] and anti-platelet treatment [13], have been demonstrated to suppress IMT progression. However, it has also been reported that IMT is not affected by either therapeutic interventions [14] or glycemic control [15]. These conflicting results might be attributable to a very small change in IMT, a 0.1 mm increase per decade in normal subjects. Such a small change may mask actual change due to inter-assay variations in IMT measurement. Most importantly, it is not possible to make a diagnosis of atherosclerosis until the appearance of arterial wall thickening.

We recently developed a novel non-invasive method for evaluating the movement of multiple sites in cardiac and arterial walls (3.616 measurement sites/9.0 mm × 6.4 mm) during a single heartbeat [16,17]. This innovative phased tracking method enables us to evaluate regional characteristics; the softer the site, the more easily it deforms during one heartbeat. This reflects regional elasticity. This method has already been applied to the in vivo detection of regional changes in cardiac and arterial walls [18–20], and the interventricular septum [21]. Evaluation of plaque vulnerability has also been attempted [16]. It is theoretically possible to detect qualitative changes in the carotid arterial wall with this method. We therefore tested the possibility of being able to detect atherosclerosis in the early stage.

Herein, we show that carotid artery elasticity, as measured in Japanese subjects with type 2 diabetes, correlates well with results obtained with currently established methods for evaluating atherosclerosis. Most importantly, elasticity correlates with the number of risk factors for atherosclerosis in those with IMT <1.1 mm, who are classified as not having atherosclerosis as defined by IMT criteria [22,23]. These results strongly suggest that it is possible to detect early stage atherosclerosis with this novel method.

2. Methods

2.1. Study subjects

The study subjects were recruited from among patients followed at the diabetes clinic at Tohoku University Hospital. Patients with type 1 diabetes, renal failure (serum creatinine >2.0 mg/dl), severe heart failure (NYHA functional class 2–4), atrial fibrillation and peripheral arterial disease were excluded from the study. All participants analyzed were Japanese type 2 diabetes patients ($n = 242$) who met the WHO criteria for diabetes mellitus. The study protocol was approved by the Tohoku University Institutional Review Board. Informed consent was obtained from each patient. Subjects characteristics are shown in Table 1.

Table 1
Subject characteristics

Number	242
Age (years)	62.1 ± 12.4
Male (%)	54.1
Body weight (kg)	62.2 ± 13.6
BMI (kg/m^2)	24.2 ± 4.2
Duration of diabetes (years)	12.0 ± 9.70
Fasting blood glucose (mg/dl)	141 ± 32.1
HbA1c (%)	7.08 ± 1.33
Systolic blood pressure (mmHg)	130 ± 18.3
Diastolic blood pressure (mmHg)	75.8 ± 11.1
Total cholesterol (mg/dl)	191 ± 38.4
HDL cholesterol (mg/dl)	51.2 ± 14.6
LDL cholesterol (mg/dl)	115 ± 31.9
Triglyceride (mg/dl)	127 ± 94.1
Uric acid (mg/dl)	5.09 ± 1.37
High-sensitive CRP (mg/dl)	0.18 ± 0.23
Diabetic retinopathy (%)	30.2
Microalbumiuria or proteinuria (%)	38.8
Diabetic neuropathy (%)	46.4
Diet:OHA:insulin (%)	20.0:37.8:42.2
Hyperlipidemia (%)	37.2
Hypertension (%)	39.3
Current smoker (%)	30.6
BMI >25 (%)	38.0

Data are presented as means ± S.D.

We used the following criteria for atherogenic risk factors. Hyperlipidemia was defined as total cholesterol ≥5.7 mmol/dl (220 mg/dl) and/or triglyceride ≥1.7 mmol/l (150 mg/dl), based on the definition proposed by the Japan Atherosclerosis Society in 2002, or taking antihyperlipidemic drugs. The subjects whose systolic BP ≥140 mmHg and/or diastolic BP ≥90 mmHg (The Japanese Society of Hypertension guidelines in 2004) or who were taking antihypertensive drugs were defined as having hypertension. The subjects who currently smoked were classified as current smokers.

2.2. Measurement of ABI and baPWV

Ankle brachial pressure index (ABI) and brachial ankle pulse wave velocity (baPWV) were measured using an automatic waveform analyzer (BP-203RPE; Colin Co., Komaki, Japan) after a 5 min rest. This device was designed to simultaneously measure blood pressure levels in both arms (brachial arteries) and ankles (posterior tibial arteries), and to then calculate the ankle systolic BP/brachial systolic BP. Pulse waves were recorded on the right brachial artery and both posterior tibial arteries. The average baPWV was calculated by divid-

ing the arm–ankle distance by the pulse wave transmission time between these points.

2.3. Measurement of carotid artery intima-media thickness

Intima-media thickness of the carotid arteries was measured using ultrasound diagnostic equipment (EUB-450, Hitachi Medico, Tokyo, Japan) with an electrical linear transducer (mid-frequency of 7.5 MHz). The common carotid artery (CCA), carotid bulb and portions of the internal and external carotid arteries on both sides were scanned with the subject in the supine position. The scan encompasses the region between 30 mm proximal to the beginning of the dilation of the bifurcation bulb and 15 mm distal to the CCA flow divider. We defined the max IMT as the thickest IMT in the scanned regions [24] and a max IMT <1.1 mm was considered normal. We defined a plaque, a focal IMT thickening, as an area with IMT ≥1.1 mm and calculated the plaque score (PS) by totaling the maximal thickness values of all plaques in the scanned area [25]. The scans were performed by a trained sonographer and the scanning period averaged 20 min in each patient.

2.4. Measurement of arterial wall elasticity

Real-time measurement of regional elasticity in the carotid artery wall was achieved based on a previously described method [20] with ultrasound diagnostic equipment (prototype system by Panasonic). With this system, an ultrasound beam is used for sequential scanning at 32 positions with a linear type 7.5 MHz probe. Multiple points were preset from the luminal surface to the adventitia along each beam with constant intervals of 320 μm, and multiple layers were defined as being between two neighboring points. Then, the displacement of each point preset along each beam was obtained by applying the phased tracking method to the received echo. Minute changes in the thickness of each layer were determined by subtracting displacements of two neighboring points. The elasticity of each layer was obtained from the thickness change and the blood pressure measured at the upper arm. Since the reflected ultrasound was resampled at an interval of 107 ns (=80 μm along the depth direction) after quadrature demodulation, we further divided each layer with a thickness of 320 μm into four points, shifted the initial depth of each layer by one-fourth of 320 μm, and applied the above procedure to each depth. Thus, the elasticity was obtained at intervals of 80 μm in the depth direction and 200 μm in the axial direction of the artery. A cross-sectional image and the process of elasticity measurement are schematically depicted in Fig. 1.

2.5. Statistical analysis

Variables were compared using Pearson's regression analysis and Student's *t*-test as appropriate. Then, a multiple linear regression analysis was performed to evaluate the independent parameters that were significantly related to arterial elasticity. The relationships between number of risk factors and the values of atherosclerosis markers were examined by analysis of covariance (ANCOVA), adjusted with age as a covariate. A p value less than 0.05 was accepted as indicating statistical significance. All statistical analyses were performed using the Statistical Package for the Social Sciences Version 13.0 (SPSS Japan Inc., Tokyo, Japan).

3. Results

We assessed the associations of carotid artery elasticity with subject characteristics (Table 2). Elasticity correlated

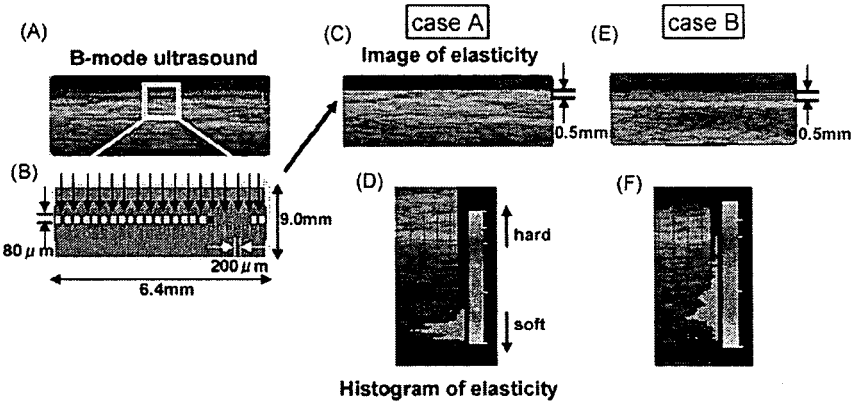

Fig. 1. The intima–media complex was visualized by conventional B-mode scanning (A), and minute thickness changes in the layers at each depth (113 depths × 32 beams per 9 mm × 6.4 mm scanned area) during one heart beat were then recorded by the phased tracking method (B). Thickness changes in each layer represent deformity, a reflection of elasticity. This elasticity is displayed as a 2D cross-sectional color image on B-mode scanning, and the image is updated at every heartbeat (C). The elasticity distribution is shown as a histogram (D). Representative results obtained from a normal subject, case A (male, age 40), are shown. Case B (male, age 45), in marked contrast, suffered from type 2 diabetes, hyperlipidemia and an old cerebral infarction, but had an IMT of only 0.5 mm, the same thickness as that of case A. The elasticity (E) was, however, extremely different from that of case A, as shown in the histogram (F).

Table 2
Associations between arterial elasticity and subject characteristics

Variables	r-Value	p-Value
Age	0.34	<0.01
Duration of diabetes	0.136	<0.05
Fasting blood glucose	−0.012	0.86
HbA1c	−0.003	0.97
Total cholesterol	0.103	0.10
HDL cholesterol	0.066	0.31
LDL cholesterol	0.089	0.17
Triglyceride	−0.064	0.32
Systolic blood pressure	0.443	<0.01
Diastolic blood pressure	0.147	<0.05
Uric acid	−0.03	0.65
High-sensitive CRP	0.037	0.56

Table 3
Mean arterial elasticity values in the presence and absence of cardiovascular risk factors

Variables	Elasticity (kPa)		p
	−	+	
Male	51.6 ± 12.6	51.0 ± 14.5	0.99
Hyperlipidemia	49.8 ± 12.3	54.7 ± 13.7	<0.01
Hypertension	49.6 ± 13.3	54.8 ± 13.6	<0.01
Current smoker	51.6 ± 13.3	51.8 ± 14.5	0.88
BMI >25	51.6 ± 13.7	51.6 ± 13.5	0.99
Diabetic retinopathy	52.3 ± 13.7	50.9 ± 14.1	0.67
Diabetic nephropathy	50.5 ± 13.6	53.9 ± 13.6	0.06
Diabetic neuropathy	50.8 ± 12.9	51.4 ± 14.4	0.65

Data are presented as means ± S.D.

Table 4
Multivariate adjustment for parameters related to arterial elasticity

Variables	Coefficient (β)	95% CI	p-Value
Age (years)	0.28	0.18–0.43	<0.01
Duration of diabetes (years)	−0.02	−0.18–0.14	0.77
Systolic blood pressure (mmHg)	0.39	0.21–0.38	<0.01
Hyperlipidemia	0.11	0.08–6.24	<0.05

with age ($r = 0.340$, $p < 0.01$), duration of diabetes ($r = 0.136$, $p < 0.05$) and blood pressure, both systolic ($r = 0.430$, $p < 0.01$) and diastolic ($r = 0.147$, $p < 0.05$).

We then examined whether or not cardiovascular risk factors affect arterial elasticity values (Table 3). Hyperlipidemic subjects had significantly higher arterial elasticity values than those with normal lipid profiles. Similarly, subjects with hypertension had higher values. However, arterial elasticity values did not depend on other risk factors, such as sex, obesity, smoking and diabetic complications.

To elucidate the independent variables affecting arterial elasticity, we performed multiple linear regression analysis with parameters related to elasticity. We employed four clinical parameters, age, duration of diabetes, systolic blood pressure and hyperlipidemia, based on the results shown in Tables 2 and 3. We found age, systolic blood pressure and hyperlipidemia to be independently associated with elasticity values (Table 4).

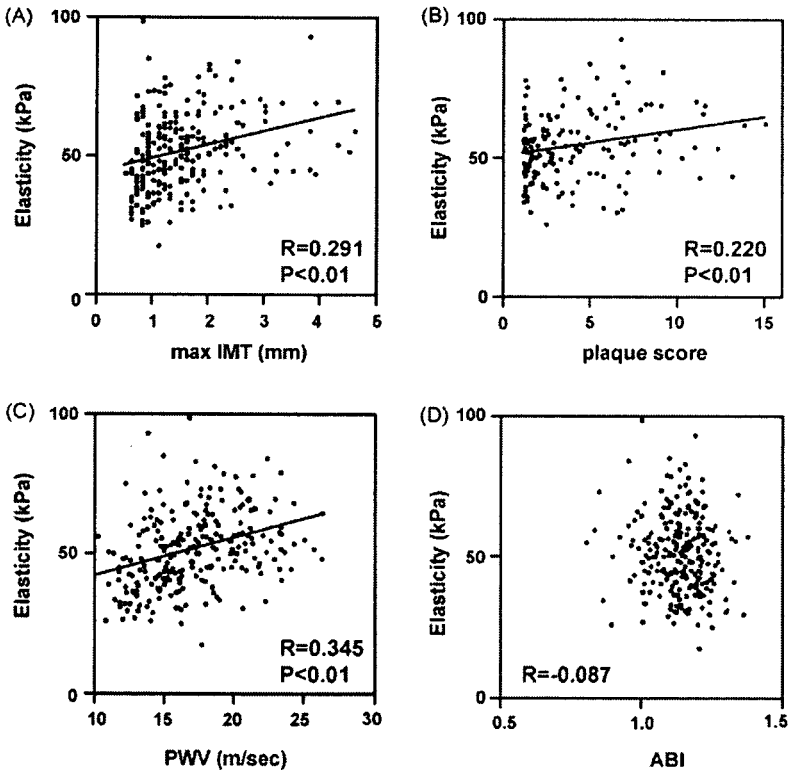

Fig. 2. Correlations between arterial elasticity values and max IMT (A), plaque score (B), baPWV (C) and ABI (D).

To assess the clinical relevance of carotid artery elasticity, we compared our elasticity values to those obtained with currently established methods for evaluating atherosclerosis: max IMT, plaque score, baPWV and ABI. Carotid artery elasticity showed significant positive correlations with max IMT ($r=0.291$, $p<0.01$) (Fig. 2A), the plaque score ($r=0.220$, $p<0.01$, $n=160$) (Fig. 2B) and baPWV ($r=0.345$, $p<0.01$) (Fig. 2C) in subjects with type 2 diabetes. It should be kept in mind that the plaque score can be obtained only in subjects with IMT ≥ 1.1 mm ($n=160$), such that the correlation was studied only in those having definite atherosclerosis based on IMT criteria [22,23]. Arterial elasticity showed no correlation with the ABI value ($r=-0.087$, $p=0.176$) (Fig. 2D). However, when we performed multiple linear regression analysis adjusted with independent parameters, age, systolic blood pressure and hyperlipidemia (Table 4), the correlations between elasticity and atherosclerosis markers (max IMT, plaque score and baPWV) were no longer present.

In a subject with more than one risk factor, the atherosclerotic process would be accelerated and thus affect the values of atherosclerosis markers. Four modifiable risk factors, diabetes, hypertension, hyperlipidemia and current smoking,

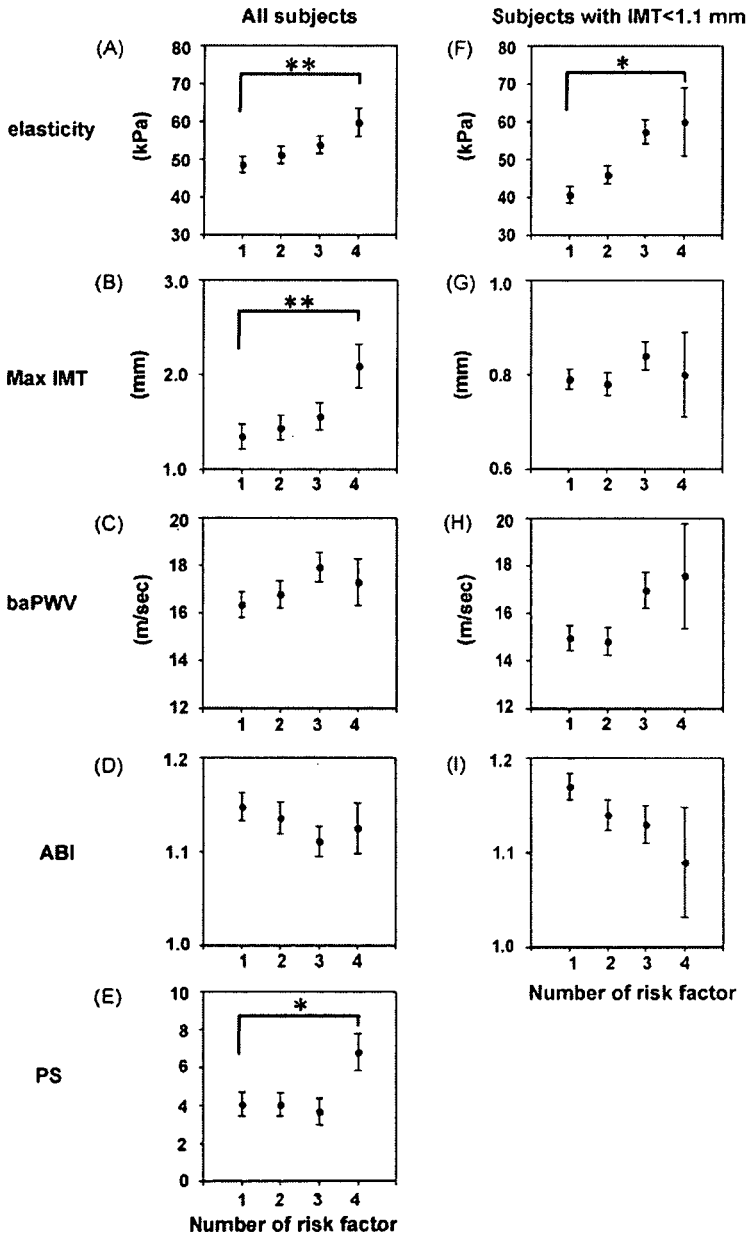

Fig. 3. Correlations of values reflecting atherosclerosis with the number of risk factors in all study subjects (A–E, $n=242$) and subjects with max IMT <1.1 mm (F–I, $n=82$). Data are presented as means ± S.E. $^{*}p<0.05$, $^{**}p<0.01$.

were taken into account in this study. All subjects had at least one risk factor, diabetes. When all the subjects were analyzed by ANCOVA, adjusted with age as a covariate, the higher the number of risk factors, the greater the attenuation of arterial elasticity values, max IMT and the plaque score (Fig. 3A, B, E). However, very interestingly, when subjects with max IMT <1.1 mm, who are regarded as not having atherosclerosis based on IMT criteria, were analyzed ($n = 82$), only age-adjusted carotid artery elasticity correlated with an increasing number of risk factors (Fig. 3F). Other age-adjusted parameters for evaluating atherosclerosis, max IMT, baPWV and ABI, showed no significant correlations with a greater number of risk factors in subjects with max IMT <1.1 mm (Fig. 3G–I).

4. Discussions

Our most important finding is that in subjects with max IMT <1.1 mm, who are regarded as being free of atherosclerosis based on IMT criteria [22,23], only carotid artery elasticity as measured with our novel non-invasive method correlated with an increasing number of risk factors. No other values obtained with the currently available methods showed correlations with the number of risk factors in these "non-atherosclerotic" subjects. Thus, our novel method of measuring arterial wall elasticity raises the possibility of detecting atherosclerosis in its early stage.

Carotid artery elasticity correlates well with results obtained with currently established methods for evaluating atherosclerosis in subjects with type 2 diabetes. These results strongly suggest that elasticity as measured with our current method reflects the severity of atherosclerosis. The measurement procedures are relatively simple, essentially the same as those of B-mode ultrasonography. In addition, arterial wall elasticity is shown as a color coded cross-sectional image with a side by side B-mode ultrasonogram, which is very practical in the clinical setting.

This novel ultrasonic method accurately tracks the movement of the arterial wall based on both the phase and the magnitude of demodulated signals, allowing instantaneous determination of the position of an object. With this method, it is possible to accurately detect small-amplitude velocity signals, less than a few micrometers, that are superimposed on arterial wall motion due to the heartbeat. This method thus allows the elasticity, a qualitative feature, of the arterial wall to be evaluated. In addition to detecting the early stage atherosclerosis, this method may enable us to evaluate progression or regression of atherosclerosis in a much shorter time than currently available methods. This possibility is extremely interesting because a means of evaluating whether or not a treatment is effective for preventing atherosclerosis is urgently needed. It usually takes years to detect the progression or regression of atherosclerosis, while it may take only months with our present method of qualitative arterial wall measurement. For example, it may be possible to detect an improvement in response to statin treatment within a few months. Similarly, we will be able to assess the effects on atherosclerosis of altering risk factors within months. These possibilities clearly merits further study.

A variety of methods are widely used for evaluating atherosclerosis. Measuring carotid IMT with ultrasound is one of the most well-established methods because it is safe, non-invasive, reproducible and easy to perform. IMT provides quantitative information, i.e. vessel-wall thickness. Depicting changes in IMT is thus generally thought to take a long time. baPWV is also a non-invasive method, which assesses atherosclerosis, as a reflection of arterial stiffness, and the usefulness of baPWV has been reported in clinical studies [26–28]. However, the pulse wave velocity depends on the ratio of the inner radius of the artery to wall thickness, which is not related to regional elasticity. It also reportedly depends on heart rate [29].

While the elasticity average of the intima and media of the carotid artery wall was calculated and used for evaluation of atherosclerosis in this study, another interesting aspect of elasticity is its distribution. The elasticity distribution, which is depicted in a histogram, might provide additional information regarding qualitative changes in atherosclerosis, and should be comprehensively studied in the future. In conclusion, our novel method for evaluating carotid artery wall elasticity holds promise for early detection of atherosclerosis.

Acknowledgments

This work was supported by a Grant-in-Aid for Scientific Research (17790599) to Y. Ishigaki and the 21st Century COE Programs "Innovative Therapeutic Development towards the Conquest of Signal Transduction Diseases" to Y. Oka from the Ministry of Education, Science, Sports and Culture of Japan. This work was also supported by a Grant-in-Aid for Research on Human Genome, Tissue Engineering (H17-genome-003) to Y. Oka. We thank Healthcare Business Company, Matsushita Electric Industrial Co., Ltd. (Panasonic), Yokohama, Japan for supplying the prototype elasticity measurement system for this study.

References

[1] Kannel WB, McGee DL. Diabetes and cardiovascular disease. The Framingham study. JAMA 1997;241:2035–8.
[2] O'Leary DH, Polak JF, Kronmal RA, et al. Carotid-artery intima and media thickness as a risk factor for myocardial infarction and stroke in older adults. Cardiovascular Health Study Collaborative Research Group. N Engl J Med 1999;340:14–22.
[3] Pignoli P, Tremoli E, Poli A, Oreste P, Paoletti R. Intimal plus medial thickness of the arterial wall: a direct measurement with ultrasound imaging. Circulation 1986;74:1399–406.
[4] Salonen JT, Korpela H, Salonen R, Nyyssonen K. Precision and reproducibility of ultrasonographic measurement of progression of common carotid artery atherosclerosis. Lancet 1993;341:1158–9.

[5] Bots ML, Hoes AW, Koudstaal PJ, Hofman A, Grobbee DE. Common carotid intima-media thickness and risk of stroke and myocardial infarction: the Rotterdam Study. Circulation 1997;96:1432–7.
[6] Touboul PJ, Elbaz A, Koller C, et al. Common carotid artery intima-media thickness and brain infarction: the Etude du Profil Genetique de l'Infarctus Cerebral (GENIC) case-control study. The GENIC Investigators. Circulation 2000;102:313–8.
[7] Yamasaki Y, Kawamori R, Matsushima H, et al. Atherosclerosis in carotid artery of young IDDM patients monitored by ultrasound high-resolution B-mode imaging. Diabetes 1994;43:634–9.
[8] Folsom AR, Eckfeldt JH, Weitzman S, et al. Relation of carotid artery wall thickness to diabetes mellitus, fasting glucose and insulin, body size, and physical activity. Atherosclerosis Risk in Communities (ARIC) Study Investigators. Stroke 1994;25:66–73.
[9] Kawamori R, Yamasaki Y, Matsushima H, et al. Prevalence of carotid atherosclerosis in diabetic patients. Ultrasound high-resolution B-mode imaging on carotid arteries. Diabetes Care 1992;15:1290–4.
[10] Minamikawa J, Tanaka S, Yamauchi M, Inoue D, Koshiyama H. Potent inhibitory effect of troglitazone on carotid arterial wall thickness in type 2 diabetes. J Clin Endocrinol Metab 1998;83:1818–20.
[11] Furberg CD, Adams Jr HP, Applegate WB, et al. Effect of lovastatin on early carotid atherosclerosis and cardiovascular events. Asymptomatic Carotid Artery Progression Study (ACAPS) Research Group. Circulation 1994;90:1679–87.
[12] Lonn E, Yusuf S, Dzavik V, et al. Effects of ramipril and Vitamin E on atherosclerosis: the study to evaluate carotid ultrasound changes in patients treated with ramipril and Vitamin E (SECURE). Circulation 2001;103:919–25.
[13] Kodama M, Yamasaki Y, Sakamoto K, et al. Antiplatelet drugs attenuate progression of carotid intima-media thickness in subjects with type 2 diabetes. Thromb Res 2000;97:239–45.
[14] Beishuizen ED, van de Ree MA, Jukema JW, et al. Two-year statin therapy does not alter the progression of intima-media thickness in patients with type 2 diabetes without manifest cardiovascular disease. Diabetes Care 2004;27:2887–92.
[15] Rantala AO, Paivansalo M, Kauma H, et al. Hyperinsulinemia and carotid atherosclerosis in hypertensive and control subjects. Diabetes Care 1998;21:1188–93.
[16] Kanai H, Hasegawa H, Ichiki M, Tezuka F, Koiwa Y. Elasticity imaging of atheroma with transcutaneous ultrasound: preliminary study. Circulation 2003;107:3018–21.
[17] Hasegawa H, Kanai H, Hoshimiya N, Koiwa Y. Evaluating the regional elastic modules of a cylindrical shell with nonuniform wall thickness. J Med Ultrason 2004;31:81–90.
[18] Kanai H, Sato M, Koiwa Y, Chubachi N. Transcutaneous measurement and spectrum analysis of heart wall vibrations. IEEE Trans Ultrason Ferroelectr Freq Control 1996;43:791–810.
[19] Kanai H, Koiwa Y, Zhang J. Real-time measurement of local myocardium motion and arterial wall thickening. IEEE Trans Ultrason Ferroelectr Freq Control 1999;46:1229–41.
[20] Hasegawa H, Kanai H, Hoshimiya N, Chubachi N, Koiwa Y. Accuracy evaluation in the measurement of a small change in the thickness of arterial walls and the measurement of elasticity of the human carotid artery. Jpn J Appl Phys 1998;37:3101–5.
[21] Kanai H, Hasegawa H, Chubachi N, Koiwa Y, Tanaka M. Noninvasive evaluation of local myocardinal thickening and its color-coded imaging. IEEE Trans Ultrason Ferroelectr Freq Control 1997;44:752–68.
[22] Salonen R, Seppanen K, Rauramaa R, Salonen JT. Prevalence of carotid atherosclerosis and serum cholesterol levels in eastern Finland. Arteriosclerosis 1988;8:788–92.
[23] Poli A, Tremoli E, Colombo A, et al. Ultrasonographic measurement of the common carotid artery wall thickness in hypercholesterolemic patients. A new model for the quantitation and follow-up of preclinical atherosclerosis in living human subjects. Atherosclerosis 1988;70:253–61.
[24] O'Leary DH, Polak JF, Kronmal RA, et al. Distribution and correlates of sonographically detected carotid artery disease in the Cardiovascular Health Study. The CHS Collaborative Research Group. Stroke 1992;23:1752–60.
[25] Handa N, Matsumoto M, Maeda H, et al. Ultrasonic evaluation of early carotid atherosclerosis. Stroke 1990;21:1567–72.
[26] Lehmann ED, Hopkins KD, Gosling RG. Increased aortic stiffness in women with NIDDM. Diabetologia 1996;39:870–1.
[27] Farrar DJ, Green HD, Wagner WD, Bond MG. Reduction in pulse wave velocity and improvement of aortic distensibility accompanying regression of atherosclerosis in the rhesus monkey. Circ Res 1980;47:425–32.
[28] Lehmann ED, Riley WA, Clarkson P, Gosling RG. Non-invasive assessment of cardiovascular disease in diabetes mellitus. Lancet 1997;350(Suppl. 1):SI14–9.
[29] Lantelme P, Mestre C, Lievre M, Gressard A, Milon H. Heart rate: an important confounder of pulse wave velocity assessment. Hypertension 2002;39:1083–7.

Available online at www.sciencedirect.com
ScienceDirect
Pharmacology & Therapeutics 117 (2008) 188–198
Pharmacology & Therapeutics
www.elsevier.com/locate/pharmthera

Associate editor: I. Kimura

Inter-organ metabolic communication involved in energy homeostasis: Potential therapeutic targets for obesity and metabolic syndrome

Tetsuya Yamada [a], Yoshitomo Oka [a], Hideki Katagiri [b,*]

[a] *Division of Molecular Metabolism and Diabetes, Tohoku University Graduate School of Medicine, 2-1 Seiryo-machi, Aoba-ku, Sendai 980-8575, Japan*
[b] *Division of Advanced Therapeutics for Metabolic Diseases, Center for Translational and Advanced Animal Research, Tohoku University Graduate School of Medicine, 2-1 Seiryo-machi, Aoba-ku, Sendai 980-8575, Japan*

Abstract

The global rate of obesity is rising alarmingly, exerting a major adverse impact on human health by increasing the prevalences of disorders, such as diabetes, hypertension and heart disease. To maintain systemic energy homeostasis, metabolic information must be communicated among organs/tissues. Obesity-related disorders can be thought of as resulting from dysregulation of this vital inter-tissue communication. Remarkable advances in obesity research during this decade have shown humoral factors manufactured and secreted by adipose tissue (adipocytokines) to be of great importance. In addition to these humoral factors, such as nutrients (glucose, fatty acids and amino acids) and hormones (insulin, adipocytokines and so on), the functional significance of the autonomic nervous system has recently attracted research attention. Autonomic nerves are essential components of the endogenous system for maintaining energy homeostasis, making them potential therapeutic targets for obesity-related disorders. This review focuses on the therapeutic possibilities of targeting inter-organ communication systems.

Keywords: Obesity; Metabolic syndrome; Inter-organ communication; Energy homeostasis; Autonomic nervous system; Central nervous system

Contents

1. Introduction

The incidence of obesity, a major risk factor for numerous disorders, including diabetes, hypertension and heart disease, is rising at an alarming rate in much of the world (Flier, 2004). Body weight is generally accepted to be determined by the balance between energy intake and expenditure. Normal weight individuals are reportedly protected against the expansion of body fat stores induced by overfeeding (Leibel et al., 1995), indicating the existence of biological mechanisms which protect against weight gain, as well as weight loss,

* Corresponding author. Tel./fax: +81 22 717 8228.
E-mail address: katagiri@mail.tains.tohoku.ac.jp (H. Katagiri).

0163-7258/$ - see front matter © 2007 Elsevier Inc. All rights reserved.
doi:10.1016/j.pharmthera.2007.09.006

at least in normal weight individuals. Energy homeostasis, maintained by multiple mechanisms, involves collecting information on systemic nutritional status and responding appropriately, both behaviorally and metabolically, to changes in fuel availability. Humoral factors, including insulin and adipocytokines, are known to be very important for this inter-organ/tissue communication. In addition, we and other investigators have recently demonstrated the autonomic nervous system to have a key role in transmitting metabolic information. Employing these systems, the brain gathers information on peripheral metabolic status, processes it, and then sends signals which regulate metabolism in the periphery. The hypothalamus, in particular, is a primary site of convergence and integration for redundant energy status signaling, which encompasses both central and peripheral neural inputs as well as hormonal and nutritional factors. These inter-tissue communication pathways are summarized in (Fig. 1; Yamada & Katagiri, 2007).

All but the most severe obesity cases can be successfully managed, solely through lifestyle modifications, i.e., improvements in diet and promotion of greater physical activity. However, low compliance with these strategies has generated interest in alternative effective therapies, including gastrointestinal bypass surgery (efficacious and long-lasting, but limited in use because of associated risks and costs) and pharmacological interventions. The market for safe and efficacious drugs is therefore potentially enormous, though the value of currently approved therapies does not reflect this potential, due to the limited efficacies and side-effect profiles of these treatments. This review summarizes our current understanding of the roles of inter-tissue communication in energy homeostasis and suggests potential therapeutic targets for obesity and the metabolic syndrome.

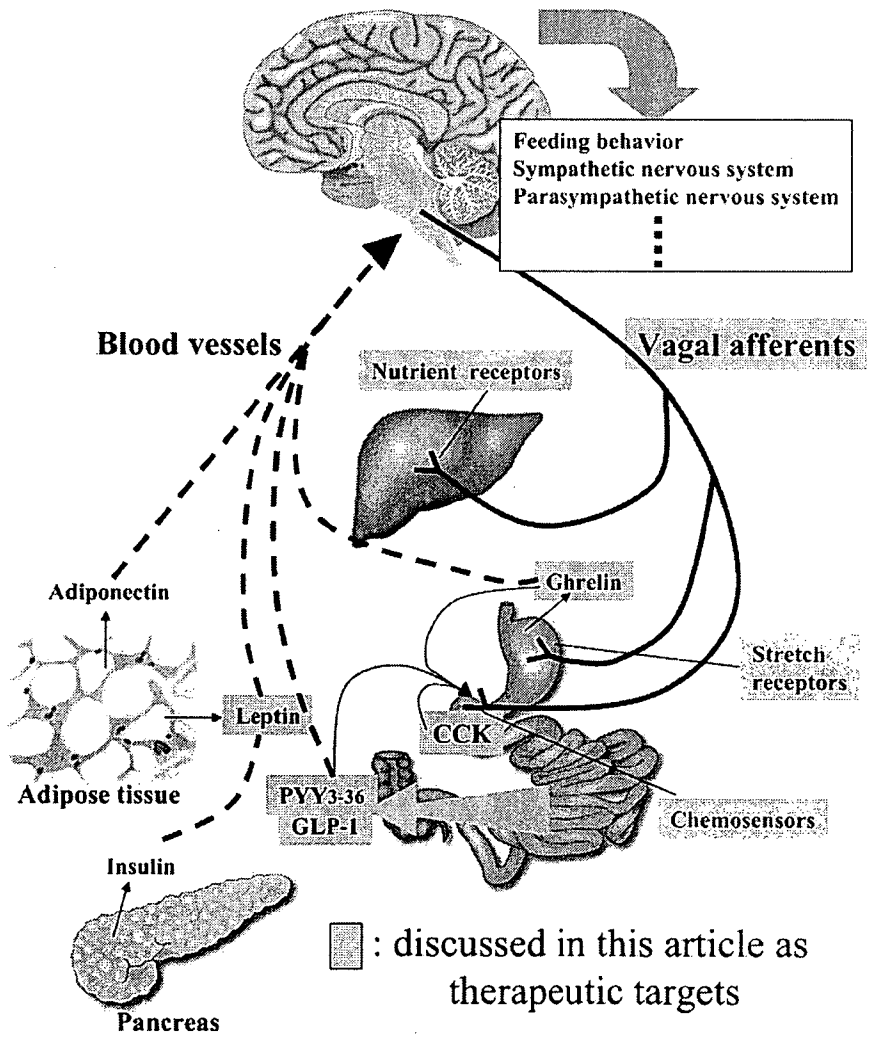

Fig. 1. Schematic presentation of intertissue communication (quoted with slight modification from Yamada & Katagiri, 2007). The brain receives various forms of metabolic information from peripheral organs/tissues through humoral and neuronal pathways. These inputs are probably integrated and processed in the brain, leading to appropriate systemic responses. Several signals, as therapeutic targets, are discussed in this article.

2. Neuroendocrine regulation of body weight and therapeutic implications for obesity

2.1. Brain inputs — humoral factors

2.1.1. Nutrients

The brain senses and then responds to nutrient-related signals arising from changes in intracellular energy contents or in either the availability or metabolism of substrates, such as free fatty acids. Some of these signals are generated in response to decreases in substrates, while others represent responses to nutrient excesses.

2.1.1.1. Glucose. In addition to serving as the primary fuel source for the brain, glucose metabolism in a subset of neurons (so-called "glucose-responsive" and "glucose-sensitive" neurons) generates signals that regulate membrane potential and neuronal firing. In glucose-responsive neurons, the molecular mechanism underlying this glucose effect resembles that, whereby glucose stimulates insulin secretion from pancreatic β cells, resulting in increased firing rates (Rowe et al., 1996). Such neurons have been characterized mainly in the ventromedial hypothalamic (VMH) nucleus and the arcuate (ARC) nucleus (Levin et al., 2004). Glucose metabolism in these cells activates KATP channels, allowing K^+ efflux, and thereby hyperpolarize the cells. KATP channel activity is a key step in converting metabolic changes into the electrical activity of ARC and VMH neurons (Wang et al., 2004). Interestingly, KATP channel activation by glucose in ARC glucose-responsive neurons is attenuated by insulin and leptin via a phosphatidylinositol 3OH kinase (PI3K)-dependent mechanism (Spanswick et al., 2000). Neither the underlying mechanism nor the extent to which these glucose-sensing neurons contribute to the actions of insulin and leptin, in neuroendocrine control of energy homeostasis, has as yet been determined.

In contrast, in glucose-sensitive neurons, firing is suppressed by glucose (Levin et al., 1999). Membrane potential effects mediated by tandem-pore K^+ (K_{2P}) channels were recently reported to be involved in glucose-induced inhibition of orexin neurons, a subset of glucose-sensitive neurons (Burdakov et al., 2006). In these neurons (in this case), glucose metabolism to ATP is not required. Thus, several types of potassium channels, including KATP and K_{2P} channels, are likely to play important roles in glucose sensing in a variety of neurons. However, the molecular mechanisms by which glucose suppresses firing in glucose-sensitive neurons is still largely unknown.

2.1.1.2. Free fatty acids. The access of circulating free fatty acids to cerebrospinal fluids is generally proportional to the plasma fatty acid concentration (Miller et al., 1987; Rapoport, 1996), indicating the brain to possibly acquire information about the peripheral metabolic state via cerebrospinal fluid fatty acid levels. Fatty acid-sensitive neurons have been identified in the hypothalamus. As an example, an *in vitro* patch clamp study (Wang et al., 2006) demonstrated 13% of arcuate neurons to show increased electrical activity, while 6% showed decreased activity, when oleic acid was applied. Several recent studies have examined the role of cerebrospinal fluid fatty acids in energy metabolism. Intracerebroventricular (i.c.v.) administration of oleic acid reportedly inhibits both hepatic glucose production and food intake (Obici et al., 2002). In addition, hypothalamic inhibition of carnitine/palmitoyl-coenzyme A transferase-1 (CPT-1), an important mitochondrial enzyme for transfer of long-chain fatty acyl-coenzyme A (LCFA-CoA) into mitochondria, decreases food intake and suppresses endogenous glucose production (EGP) in the liver (Obici et al., 2003). Efferent vagal nerve signals from the brain to the liver are also reportedly involved in hepatic gluconeogenesis in these experimental settings (Pocai et al., 2005a, 2005b). Hu et al. found that central administration of C75, a potent fatty acid synthase (FAS) inhibitor, decreased food intake (Hu et al., 2003). Since FAS inhibition increases malonyl-CoA and thereby suppresses CPT1 activity, LCFA-CoA in hypothalamic neurons would appear to be increased. These results, taken together, indicate the cytoplasmic LCFA-CoA concentration in hypothalamic neurons to play an important role in energy homeostasis. Further studies are needed to clarify the mechanisms regulating the neuronal LCFA-CoA content, its relationship to plasma free fatty acid (FFA) levels and the intracellular mechanism whereby a change in the LCFA-CoA content alters neuronal function.

2.1.1.3. Amino acids. Amino acids also apparently transmit energy status information from the periphery. Amino acids are reportedly transported across the blood–brain barrier (Choi et al., 2001). Therefore, the amino acid levels in cerebrospinal fluids appear to reflect those in peripheral blood. Centrally administered leucine increases hypothalamic mammalian target of rapamysin (mTOR) activity, thereby decreasing both food intake and body weight (Cota et al., 2006). mTOR is a highly conserved serine/threonine kinase found in organisms from yeast to mammals. mTOR activity sensitive to branched chain amino acid levels, especially that of L-leucine (Proud, 2002; Meijer & Dubbelhuis, 2004). Thus, mTOR is known to be among the energy sensors for amino acids conserved throughout evolution and, in mammals, hypothalamic mTOR signaling apparently plays an important role in regulating systemic energy metabolism. Leptin increases hypothalamic mTOR activity, and inhibition of mTOR signaling suppresses leptin's anorectic effect (Cota et al., 2006). However, further studies are needed to fully clarify mTOR's role in energy homeostasis.

2.1.2. Hormonal signals

2.1.2.1. Insulin. Insulin, produced by pancreatic β cells, is the master metabolic switch between fed and fasted states, mediating metabolic fuel disposition and use. Some investigators speculate that insulin itself might signal fuel status to the brain, but the actual mechanisms by which insulin would exert such effects have long eluded clarification.

An electrophysiological study showed inhibitors of PI3K to block the capacity of insulin to hyperpolarize hypothalamic "glucose-responsive" neurons (Spanswick et al., 2000). A subsequent in vivo study showed i.c.v. infusion of PI3K inhibitors to effectively prevent insulin-induced anorexia (Niswender et al., 2003). Furthermore, activation of insulin signaling in the ARC

alone, in the absence of elevated systemic insulin, is sufficient to decrease not only food intake but also blood glucose levels, by markedly inhibiting EGP in the liver (Plum et al., 2006; Prodi & Obici, 2006). A recent study revealed the central effects of insulin on this hepatic EGP suppression to be mediated by KATP channel activation through the insulin receptor (IR)–insulin receptor substrate 2 (IRS2)–PI3K pathway in the ARC (Pocai et al., 2005a, 2005b). Thus, intracellular insulin signal transduction in the brain, particularly in the hypothalamic ARC nucleus, plays an important role in regulating food intake, as well as in systemic glucose metabolism.

2.1.2.2. Leptin. Leptin was identified by positional cloning using the *ob/ob* mouse model (Zhang et al., 1994) as a key molecule in the regulation of both body weight and energy balance. Leptin is produced mainly by adipocytes in proportion to fat stores. Adipocyte leptin expression is transcriptionally regulated, being determined mainly by adipocyte size. Adequate leptin levels communicate the status of energy stores in white adipose tissue (WAT) to the central nervous system (especially the hypothalamus), suppressing food intake and permitting energy expenditure via sympathetic stimulation of several tissues (Haynes et al., 1997; Friedman & Halaas, 1998). As an example, when energy stores increase, the energy balance is negatively regulated by decreased food intake and increased energy expenditure (Friedman & Halaas, 1998). Leptin binds to the leptin receptor Ob-Rb in the hypothalamus, thereby activating the JAK-STAT (Bjorbaek et al., 1997; Bates & Myers, 2004) and IRS2-PI3K (Niswender et al., 2001) pathways. Leptin also suppresses hypothalamic AMPK activity and thus reduces food intake (Minokoshi et al., 2004). As described above, leptin also activates mTOR signaling in the hypothalamus. Thus, there appear to be complicated interactions among the (at least) 4 pathways, JAK-STAT, IRS2-PI3K, AMPK and mTOR, involved in leptin signaling.

In most individuals with ordinary obesity, circulating leptin is elevated, but the body does not adequately respond to higher leptin levels by reducing food intake. This lack of responsiveness to leptin in most forms of obesity raises the possibility that obesity is a state of relative leptin resistance. Leptin resistance is thought to be an important mechanism for maintaining the obese state.

2.2. Brain inputs — afferent nerve signals

2.2.1. Innervation

2.2.1.1. Intra-abdominal innervation without white adipose tissues. Innervation of intra-abdominal tissues warrants an explanation. Intra-abdominal tissues are innervated by both splanchnic (sympathetic) and vagal (parasympathetic) nerves. These nerve bundles consist of both efferent and afferent fibers. Detailed fiber count studies have revealed abdominal vagal and splanchnic nerves to be comprised of approximately 75% and 50% afferent fibers, respectively. Vagal afferents respond to specific chemical stimuli, the degree of physiological gut distention and nutrients, whereas splanchnic afferents carry information about noxious stimuli (Badman & Flier, 2005).

2.2.1.2. Innervation of intra-abdominal adipose tissues. WAT is also innervated by both efferent and afferent nerve fibers. Numerous reports have described the important metabolic roles, including lipolysis and β oxidation (Shimazu, 1981; Bartness & Bamshad, 1998; Imai et al., 2006), of efferent sympathetic fibers. Efferent parasympathetic innervation of WAT is controversial (Kreier et al., 2002; Giordano et al., 2006). On the other hand, afferent nerves from WAT have been demonstrated by several methods. Sensory innervation of WAT was directly demonstrated using a neuroanatomical approach with application of an anterograde tract tracer, True Blue, to WAT, resulting in labeling of neurons in rat dorsal root ganglia (Fishman & Dark, 1987). More recently, afferent innervation of epididymal WAT was demonstrated by another group using the pseudorabies virus as a retrograde neuronal tracer (Kreier et al., 2006).

2.2.2. Signals transmitted by afferent autonomic nerve fibers

2.2.2.1. Signals from the gut. Many peptides are synthesized and released by the gastrointestinal tract. Several of these peptides, such as cholecystokinin (CCK), glucagon-like peptide-1 (GLP-1), peptide YY (PYY) and ghrelin, have been shown to modulate eating behaviors, (Woods & Gibbs, 1989; Stanley et al., 2004; Woods, 2004). Several of these peptides have direct access to brain regions involved in regulating food intake, such as the ARC of the hypothalamus and the area postrema, via the circulation. These peptides also function outside the CNS, influencing the activities of neurons, e.g., the vagal afferent nerve which projects to the nucleus of the solitary tract (NTS) in the brain stem. Further research is needed to determine the weighting and integration of each of these different signals.

2.2.2.1.1. CCK. CCK, produced by mucosal enteroendocrine cells of the duodenum and jejunum, is secreted in response to the presence of food in the gut lumen. Satiating effects of CCK have been confirmed based on the carboxy-terminal octapeptide of CCK reducing meal size and duration (Pi-Sunyer et al., 1982). Pharmacologic and genetic experiments have yielded evidence that the CCK1 receptor mediates CCK-induced satiation (Moran et al., 1998; Kopin et al., 1999). Sulfated CCK, which preferentially binds to CCK1R on vagal afferent neurons, signals satiety to the brain; this explains why vagotomy inhibits the anorectic effect of CCK (Smith et al., 1981). However, CCK1R is also expressed in both the hindbrain and the hypothalamus. Lesioning the hindbrain area postrema attenuates CCK-induced satiation (Edwards et al., 1986) and CCK microinjections into several hypothalamic nuclei lead to decreased food intakes (Blevins et al., 2000). Collectively, these observations suggest that CCK might relay satiation signals to the brain both directly and indirectly.

Continuously administering intraperitoneal CCK to rats results in reduced meal sizes, but this reduction is offset by increased meal frequency, such that there is no effect on body weight (West et al., 1984). In human subjects, food intake and gastric emptying were acutely reduced by CCK infusions (Muurahainen et al., 1988), but these anorectic effects disappeared after only 24 hr of continuous infusion (Crawley & Beinfeld, 1983). Therefore, although CCK clearly plays a role in terminating individual